Contemporary hybridization among *Arabis* floodplain species creates opportunities for adaptation

Authors:

Neda Rahnamae[1,2], Lukas Metzger[3,4], Lea Hördemann[1], Kevin Korfmann[5], Abdul Saboor Khan[1], Craig I. Dent[6,7], Samija Amar[6], Raúl Y. Wijfjes[8], Tahir Ali[1], Gregor Schmitz[1], Benjamin Stich[9], Aurelien Tellier[3], Juliette de Meaux[1,*]

[1]Institute for Plant Sciences, Biocenter, Cologne, Germany

[2]Institute of Plant Ecology and Evolution, Heinrich-Heine University Düsseldorf, Düsseldorf, Germany

[3]Professorship for Population Genetics, Department of Life Science Systems, Technical University of Munich, Freising, Germany

[4]Research Department for Limnology, Mondsee, University of Innsbruck, Innsbruck, Austria

[5]Institute of Ecology and Evolution, University of Oregon, Eugene, OR, USA

[6]Department of Chromosome Biology, Max Planck Institute for Plant Breeding Research, Cologne, Germany

[7]CEPLAS: Cluster of Excellence on Plant Sciences, Heinrich-Heine University, Düsseldorf, Germany

[8]Faculty of Biology, LMU Munich, Planegg-Martinsried, Germany

[9]Julius Kühn Institute (JKI), Federal Research Centre for Cultivated Plants, Institute for Breeding Research on Agricultural Crops, Sanitz, Germany

*For correspondence (e-mail: jdemeaux@uni-koeln.de).

Abstract

Hybridization between closely related species is increasingly recognized as a major source of biodiversity. Yet, whether it can create advantageous trait combinations while purging harmful alleles remains unknown. We studied *Arabis nemorensis* and *A. sagittata*, two endangered species that currently hybridize in a single hotspot. We measured 22 phenotypic traits and mapped their genetic basis in an F2 population, after generating high quality genome

assemblies for both species. In total, 58 QTLs were identified for 20 traits, with additive and dominance effects best fitting Gaussian and logistic distributions, respectively. Six large-effect QTLs were linked to significant hybrid fitness loss. Two genomic regions showed strong transmission bias favoring *A. sagittata* alleles, potentially accelerating their introgression. However, 48% of QTLs were unlinked to reduced fitness or segregation distortion and may generate genotypes exceeding parental performance. Notably, a major QTL affecting flowering time explained 23% of phenotypic variation and implicated *TFL1* as a candidate gene for life history adaptation. While most QTLs lacked overlap with past selective sweeps, indicating limited recent positive selection, 5 of 7 QTLs for rosette size overlapped with sweep signatures in the parental lineages. Overall, our findings offer unique insights into incipient stages of hybridization.

Keywords: hybridization, QTL mapping, meiotic drive, heterozygote advantage, competitive grasslands, *Arabis* genome.

Introduction

Biodiversity is crucial for the structure and functioning of ecosystems (Staudinger *et al.*, 2012). The direct impact of human activity and the escalating threat of climate change have initiated the sixth Mass Extinction (Cochrane *et al.*, 2016; Ceballos *et al.*, 2020; Cowie *et al.*, 2022; IPCC, 2023), sparking global concern (Hooper *et al.*, 2002; Eichenberg *et al.*, 2021; Theissinger *et al.*, 2023) and prompting investigation into how species will cope (Moore & Hendry, 2009; Bontrager & Angert, 2019; Schlaepfer & Lawler, 2023). For species endangered by rapid shifts in the environment, the acquisition of pre-adapted alleles via hybridization could provide plants with a strategy to immediately combat climate change (Hansen *et al.*, 2012; Anderson *et al.*, 2012; Chunco, 2014; Brauer *et al.*, 2023).

Hybridization, the interbreeding of individuals from genetically distinct populations or species, occurs frequently among close relatives (Blanckaert *et al.*, 2023; Peñalba *et al.*, 2024; Rosser *et al.*, 2024). It can have both advantageous and detrimental consequences on the species receiving gene flow (Peñalba *et al.*, 2024). First, interspecific hybridization can enable locally adapted alleles across species barriers to be transferred and thus enhance the adaptive potential of species (Seehausen, 2004; Pfennig *et al.*, 2016; Abbott, 2017). Indeed, hybridization between populations with different ecological specializations can give rise to new, viable, and fertile hybrids equipped with novel trait combinations. Such combinations may improve the fitness of the population or even enable previously untapped habitats to be colonized (Buerkle *et al.*, 2000; Rieseberg *et al.*, 2003; Mallet, 2007; Abbott *et al.*, 2013; Blanckaert *et al.*, 2023). Because this process can contribute to the rescue of endangered

species, it may help maintain diversity, as seen in genus *Pachyclasdon*, which appears to have survived the Last Glacial Maximum thanks to genetic information transferred through hybridization in alpine refugia on New Zealand's South Island (Becker *et al.*, 2013). Early-flowering alleles of *Helianthus argophyllus* were enriched among locally adapted introgressed genomic fragments in *Helianthus* spp and *Betula platyphtylla* (Todesco *et al.*, 2020; Nocchi *et al.*, 2023). Hybrid populations between generalists and narrow range endemic rainbowfishes (*Melanotaenia* spp.) were well adapted to environmental changes thanks to the effects of introgression (Brauer *et al.*, 2023). Hybridization has even been proposed to promote the formation of new species, a phenomenon referred to as "hybrid speciation"; however, whether a new species actually results is controversial (Anderson & Stebbins, 1954; Ellstrand & Schierenbeck, 2000; Schumer *et al.*, 2015).

The detrimental effects of hybridization are often more readily detected than its advantageous effects. Indeed, allelic incompatibilities can cause a massive fitness breakdown, when gene pools reunite after long periods of evolution in isolation (e.g., *Drosophila* [Masly & Presgraves, 2007; Cooper *et al.*, 2018]; *Mimulus* [Zuellig & Sweigart, 2018]; *Mus* [White *et al.*, 2011; White *et al.*, 2012; Wang *et al.*, 2015]; *Xiphophorus* [Schumer *et al.*, 2014; Schumer & Brandvain, 2016; Powell *et al.*, 2020; Moran *et al.*, 2024]; Bomblies & Weigel, 2007; Presgraves, 2010; Coughlan & Matute, 2020; Li *et al.*, 2022). The overall fitness of the hybridizing population will be reduced if too many resources are used to produce poorly performing hybrids (Rhymer & Simberloff, 1996; Todesco *et al.*, 2016; Goulet *et al.*, 2017). This phenomenon, sometimes described as "demographic swamping," elevates the risk of extinction but may also select for allelic variations that reinforce species isolation (Hopkins, 2013; Goulet *et al.*, 2017; Ma *et al.*, 2019; Brauer *et al.*, 2023).

Despite the interest in the positive consequences of hybridization and the abundant evidence for allelic incompatibilities (Bomblies & Weigel, 2007), we know little about how the positive and negative effects of hybridization interact, much less about how a genotype carrying adaptive alleles might emerge – especially against a background in which detrimental effects have been recombined out. Such "super genotypes," although rare in the offspring of the first generation of hybrids (many of which may perform poorly), may represent new and exceptional combinations of adaptive alleles that in selfing species can determine the evolutionary success of hybridization. In addition, much focus has been placed on showing that introgressed alleles bring adaptive advantages to the recipient species (Edelman and Mallet 2021). Yet, the role that natural selection has played in shaping the introgressing alleles of the donor species has seldom been examined. Addressing these two challenges is best achieved when hybridization

can be studied as it proceeds, as this allows direct observation of the recombination and selection dynamics shaping introgressed variation.

Here, we focused on a hybridization hotspot located along the banks of the Rhine River near Mainz, Germany, where two endangered Arabis species hybridize in a floodplain meadow (Dittberner *et al.*, 2019; Dittberner *et al.*, 2022). *Arabis nemorensis*, a species within the Brassicaceae family (*Arabis hirsuta* tribe), inhabits floodplain meadows and is currently in a critical state in Central Europe, requiring special attention from conservation authorities (Schnittler & Günther, 1999; Burmeier *et al.*, 2011). *A. nemorensis* is self-pollinating and exhibits low levels of nucleotide diversity. Its endangered status is further intensified by its unique ecological requirements, and the loss of its natural habitat (Hölzel, 2005; Burmeier *et al.*, 2011; Mathar *et al.*, 2015; Dittberner *et al.*, 2019). *A. sagittata*, another member of the same phylogenetic tribe (Karl & Koch, 2014), is morphologically very similar but commonly found in calcareous grasslands and thus possibly more tolerant to drought (Dittberner *et al.*, 2022). *A. sagittata* was recently observed in floodplains, where it naturally hybridizes with *A. nemorensis* (Dittberner *et al.*, 2019; Dittberner *et al.*, 2022).

Introgression analysis has revealed that gene flow between *A. nemorensis* and *A. sagittata* has happened in the past, but contemporary hybridization is restricted to the sympatric population, where intraspecific genetic variation is extremely low (Dittberner *et al.*, 2019; Dittberner *et al.*, 2022). Additionally, population genetics analyses estimated the divergence between *A. nemorensis* and *A. sagittata* occurred around 900,000 generations ago, with practically complete isolation after the last glaciation (Dittberner *et al.*, 2022).

Using the F2 progeny of a cross between two representative genotypes of *A. nemorensis* and *A. sagittata* from the hybridizing hotspot, we addressed the following questions: (1) What are the phenotypic differences of relevant ecological traits? (2) What is the genetic architecture of interspecific differences in this hybridizing hotspot? (3) Can a new combination of ecologically relevant traits arise and establish after hybridization? (4) Do QTL regions enriched in genomic regions carry footprints of past selection? Our study confirmed the extent of the genetic differences underpinning phenotypic divergence between two species. In addition, we found that some F2 hybrids show extreme trait values, despite their generally lower seed production compared to parental lines. Interestingly, incompatibility QTLs have a simple genetic basis, and some ecologically relevant QTLs are independent from the incompatibility QTLs. Collectively, these results indicate that a few offspring of hybridized species may potentially harbor a genotype with a combination of properties that none of the parents have.

Materials and Methods

Common Garden Experiment and Phenotyping

We crossed sympatric *A. nemorensis* genotype 10 with the *A. sagittata,* genotype 69, collected from the banks of the Rhine River near Mainz in Riedstadt, Hessen, Germany in 2015 and fully sequenced (Dittberner *et al.*, 2019; Dittberner *et al.*, 2022). Because nucleotide diversity within the population is very low (*A. nemorensis* π = 4.37e-5 and *A. sagittata* π = 1.32e-5, synonymous sites, Dittberner *et al.*, 2022), we assume here that differences between these genotypes will predominantly reflect differences between species. Plants were reciprocally crossed to generate F1s, and we noted that their fitness was comparable to that of the parental species (Fig. S1). Seedlings were grown in the greenhouse of the Experimental Garden of the University of Cologne, and the seeds of the first generation of selfing (F2) were harvested. We sowed F2 seeds in trays on 05.10.2019, and after two weeks of vernalization and germination we transplanted seedlings into 7x7cm pots filled with *Topferde* soil (Einheitserde, Sinntal-Altengronau, Germany), placing one seedling per pot. In total, 1,204 individual plants (both hybrids and parental replicates) were distributed across 43 trays, which were put in cold frames to accelerate growth and prevent frost damage from 08.11 to 13.12.2018. On 13.12.2018, we transferred trays to bird-protected cages under seminatural conditions. On 19.11.2018, photographs of each tray were taken using a Canon EOS and rosette sizes were measured using ImageJ. Also, on 19.12.2018, we started harvesting leaves from plants that were big enough (~50 mg of leaves per plant). Harvesting continued in January, February, and March 2019. Harvested rosette leaves were stored at -80°C for DNA extraction.

On 01.03.2019, eight trays were moved to cold frames for a 10-day period to recover from potential stress. A total of 199 F2 individual plants, along with seven *A. nemorensis* and seven *A. sagittata*, were submerged in transparent boxes, each containing 17 L of water for seven weeks. Plants were randomized and distributed across eight boxes, which were kept in cold frames throughout the submergence experiment. After seven weeks of complete submergence, plants were removed from water and left to recover. Then, their survival status was documented. Following a two-week recovery period, we again recorded the survival status of plants, categorizing plants as either dead, survived with new leaf growth, or survived and bolted. During recovery, pots remained in cold frames and were watered as necessary.

Between November 2018 and April 2019, we recorded more than 20 phenotypic traits for each plant. These traits were grouped into five categories: (1) fitness: seed mass from 10 randomly selected siliques or fertility score and survival status after submergence; (2) growth: rosette diameter at four time points (19.11.2018, 08.01.2019, 07.02.2019, 13.03.2019), inflorescence

height, and ena of side and ground shoots; (3) timing: bolting and flowering times; (4) rosette leaf Ttraits: stem leaf number, leaf length, petiole length, lamina length, lamina length/width ratio, leaf margin type (serrated or smooth), leaf width, and petal length; and (5) stem traits: stem leaf density, stem leaf length and width, and stem height.

Phenotypic Analyses

To assess phenotypic differences between the two species, we used a generalized linear model (trait ~ Tray, with quasipoisson distribution of error) to analyze each trait, controlling for experimental effects, in R. A t-test from the stats package in R (version 3.6.2) was then applied to the residuals of the models to calculate the significance of differences (p-value < 0.05) between the two groups (*A. nemorensis* and *A. sagittata*, each with 35 replicates) for each trait. We used ggplot2 (version 3.5.1; Wickham, 2011) to visualize the distribution of phenotypes for both F2 and parental replicates in a single plot per trait, and to inform our understanding of transgressive segregation within the F2 population (Suppl. File 1).

For genetically based phenotypic correlation between individuals of the F2 population, we employed a mixed-effects model approach (trait ~ Cross/TrayBlock) that accounted for random variation attributable to experimental blocks and trays, and cross direction due to reciprocal cross. Residuals were extracted for each trait, and pairwise Spearman correlations were calculated using the *corr.test* function from the psych package in R (version 2.4.6.26); pairwise deletions were applied to handle missing data. Correlation significance was assessed at $\alpha = 0.05$. The resulting correlation and p-value matrices were used to construct a network in which only significant correlations were retained. A network graph was generated using the igraph (version 2.1.1) and ggraph (version 2.1.1) packages. Each node represents a phenotypic trait, and edges represent statistically significant pairwise correlations. Edge color indicates the sign of the correlation (green for positive, brown for negative), and edge thickness is scaled to the absolute strength of the correlation. Curved edges and partial transparency were used to enhance visual clarity, and node labels were plotted within stylized trait circles. The *ggcorrplot* function from the ggcorrplot package (version 0.1.4.1) was used to visualize the heatmap.

DNA Extraction and RAD-seq Library Construction

DNA was extracted from leaves stored at -80°C using the Nucleospin® 8 Plant II protocol. Using the restriction-site-associated DNA sequencing (RAD-seq) protocol described in Dittberner *et al.* (2019), we analyzed the genomes of 801 F2 individuals. DNA was quantified with Qubit® 3.0. Fluorometer. For each sample, a total of 250 ng of genomic DNA was

198 digested with the KpnI-HF restriction enzyme (New England Biolabs). Each digested sample
199 was then ligated with one individually barcoded modified Illumina P1 adapter containing 5 bp
200 random nucleotides to PCR duplicates to be removed in the steps that follow. Twenty different
201 barcodes were used, and 52 pools of 20 barcoded individuals each were constructed, with all
202 pools standardized to equal volume and concentration. Libraries were sequenced in four
203 separate runs at the Cologne Center for Genomics (CCG) on the Illumina NovaSeq platform.
204 For 46 pools, sequencing length was 2x100 bp, generating approximately 3 million reads per
205 individual; for the remaining 6 pools, sequencing length was 2x150 bp, generating
206 approximately 6 million reads per individual. These RADseq libraries covered, on average,
207 approximately 2% of the 248 Mb genome.

208 **Genome Assembly and Annotation**

209 In order to improve previous genome assemblies, the DNA of both parental lines was
210 sequenced with PacBio HiFi technology and Hi-C data. We used Jellyfish (version 2.3.0;
211 Marçais & Kingsford, 2011) to count k-mers of size 21 in the 2.18 and 1.98 million reads
212 obtained for *A. nemorensis* and *A. sagittata*, respectively. The k-mer histogram generated by
213 Jellyfish was then processed with GenomeScope (version 2.0; Ranallo-Benavidez *et al.*, 2020)
214 to estimate genome size, heterozygosity, and repetitiveness. HiFiAdapterFilt (version 2.0.0;
215 Sim *et al.*, 2022) was used to remove residue PacBio adapter sequences from the HiFi reads.
216 Then, hifiasm was used again to assemble the filtered HiFi reads (version 0.16.1; Cheng *et*
217 *al.*, 2021; Cheng *et al.*, 2022) with integration of Hi-C data.

218 Hi-C reads were aligned to the draft contigs using BWA (version 0.7.17; Li & Durbin, 2009),
219 and the resulting alignments were processed with the Juicer pipeline (version 1.6; Durand *et*
220 *al.*, 2016b) to generate chromatin contact maps. These maps were manually inspected and
221 curated using Juicebox (version 2.20.00; Durand *et al.*, 2016a) to correct misjoins and to
222 anchor and orient contigs into chromosome-scale scaffolds. This integration significantly
223 enhanced the contiguity and accuracy of the assembly.

224 To scaffold the primary assembly produced by hifiasm, we employed RagTag (version 2.1.0;
225 Alonge *et al.*, 2022), using the *A. alpina* assembly as a reference (Suppl. File 2) to further
226 improve scaffold ordering and correct structural inconsistencies. In addition, a linkage map
227 (see below) allowed us to correct a few minor assembly errors. The final assemblies have
228 been deposited in the European Nucleotide Archive (ENA) and is awaiting an accession
229 number (Project id: PRJEB89863). The ab-initio annotation was generated using the *A.*
230 *nemorensis* reference genome, which was uploaded to the PlabiPD Helixer platform

231 (https://www.plabipd.de/helixer_main.html). The annotation was performed in "Lineage-
232 Specific" mode with selection of the option "Land Plant".

233 **Analysis of RAD-seq Data, SNP Calling, and Construction of Linkage Map**

234 RAD-seq read quality was assessed with FastQC (version 0.11.9; Andrews, 2010). PCR
235 duplicates were removed using the clone_filter module in Stacks (version 2.59; Catchen *et al.*,
236 2013), based on a 5 bp random nucleotide sequence at the end of each adapter. Adapters
237 were trimmed and reads shorter than 60 bp were removed using Cutadapt (version 1.18;
238 Martin, 2011). We demultiplexed samples and filtered out reads with ambiguous barcodes
239 (allowing one mismatch), cut sites, uncalled bases, and low-quality reads (default threshold)
240 using the process_radtags module in Stacks (version 2.59). Reference-based mapping and
241 read-filtering were conducted with BWA (version 0.7.17; Li & Durbin, 2009) using default
242 settings against the *A. nemorensis* reference genome, along with SAMtools (version 1.10; Li
243 *et al.*, 2009) and bash scripts from Rivera-Colón & Catchen (2022) (Suppl. File 3).

244 We performed variant-calling for 801 individuals using BCFtools mpileup and call (version
245 1.18; Li *et al.*, 2009) under specific criteria: a base quality score greater than 30, base quality
246 recalculation (-E option), and SNP calling with a significance threshold of p-value < 0.05.
247 Genotyped loci were filtered using VCFtools (version 0.1.17; Danecek *et al.*, 2011) to exclude
248 loci with more than 50% missing data across individuals. Only biallelic sites were kept, and
249 indels were removed. Individuals with over 60% missing data were excluded, leaving a
250 working set of 781 individuals for subsequent analysis. Additional filters were applied to site
251 and genotype depth (--min-meanDP 4 --max-meanDP 40 --minDP 5 --maxDP 40), and sites
252 with more than 70% missing data were then removed. Loci spaced less than 100 bp apart
253 were clustered into RAD regions as described by Dittberner *et al.* (2019). Regions with
254 abnormally high or low coverage were excluded based on specific thresholds: mean coverage
255 greater than twice or less than one-third the overall mean, maximum coverage exceeding
256 twice the mean maximum coverage across all regions, or regions shorter than 150 bp. Sites
257 absent from parental lines and ambiguous bases were also removed. Finally, we applied a
258 minor allele frequency filter (--maf 0.25) to the dataset. SNPs (single nucleotide
259 polymorphisms) were extracted using VCFtools (version 0.1.17; Danecek *et al.*, 2011) and
260 custom Python scripts, resulting in a VCF file containing 5,360 SNP markers across 781
261 individuals (Suppl. File 3).

262 We applied additional filters to improve the quality of map construction. We removed 39
263 individuals with missing data exceeding 3,500 loci. Duplicated markers were identified and
264 removed, resulting in 47 markers being discarded. Subsequently, markers with more than 23%

missing data were filtered out. To analyze the remaining 2,164 markers, we examined their distribution along the genome, compared segregation distortion patterns with allelic proportion and missingness, and filtered out markers identified as outliers based on allelic proportion. We further removed markers with fractions of heterozygotes lower than 25% or higher than 75%. We also used RepeatMasker (version 4.1.6; Smit *et al.*, 2015) on genome annotations to detect and remove markers within repetitive regions. We used repeatmodeler to identifiy repeat families, an approach that was used in Repeatmasker to mask the repetitive regions in the genome. This final analysis produced a genetic map of 2,082 markers distributed across eight chromosomes for 742 individuals (Suppl. File 4).

To improve the accuracy of genotype calling, particularly for heterozygous loci located in low-coverage regions, a Python script was developed to correct incorrectly called genotypes and impute missing data using a sliding window approach. The 2 Mb window size with a 0.5 Mb step size demonstrated the most effective correction and imputation. No further markers or individuals were excluded after this correction and imputation step. The finalized corrected dataset was then used to construct the genetic map using the ASMap package in the R environment (version 1.0-7; Taylor & Butler, 2017) packages in R (version 4.2.3), applying the so-called Kosambi mapping function in the R/qtl package (version 1.66; Broman *et al.*, 2003) as detailed in Supplemental File 4.

Chromosomal orientation was assessed using the constructed genetic map, identifying inversions on chromosomes 3, 4, 6, and 7 due to assembly issues. These regions were adjusted by inverting physical distances on the genetic map, and the genome assembly was subsequently corrected. See above (Genome Assembly and Annotation) for details on the genome assembly process.

Segregation Distortion and Selection Coefficient

We assessed segregation distortion within each region by applying a test of segregation distortion (profileMark) for each marker with Bonferroni correction using the ASMap package in R. To assess deviations from the Hardy-Weinberg equilibrium (HWE) and estimate selection coefficients, allele frequencies for each genotype (NN, NS, SS) were calculated based on the total number of individuals (N = 742). The observed genotype counts were used to compute allele frequencies ($Freq_N$ and $Freq_S$) by summing homozygous and heterozygous contributions. Expected genotype frequencies under the HWE were then computed as ${Freq_N}^2$ (NN), 2 × $Freq_N$ × $Freq_S$ (NS), and ${Freq_S}^2$ (SS). These frequencies were scaled to expected counts by multiplying by the total number of individuals (Suppl. File 4).

To determine significant deviations from the HWE, a chi-squared goodness-of-fit test was performed for each locus. The observed and expected genotype counts were compared using the chi-squared statistic, with 2 degrees of freedom. Significant deviations were identified based on a Bonferroni-corrected *p*-value threshold, accounting for multiple testing across all loci. The Bonferroni correction was applied by adjusting the significance threshold to 0.05 divided by the total number of markers (2,082); this adjustment ensured that false positives were stringently controlled for. Additionally, selection coefficients (t and s) were estimated by calculating the relative differences in ratios of observed to expected frequencies among genotypes. Specifically, the coefficients were defined $s_{NN} = 1 - \frac{ratio_{NN}}{ratio_{NS}}$ and $s_{SS} = 1 - \frac{ratio_{SS}}{ratio_{NS}}$, reflecting the relative fitness difference between homozygotes and heterozygotes (Carey & Ganders, 1980) (Suppl. File 4).

Significance of genotype deviations from the HWE was assessed using a chi-squared test for each marker. *P*-values were adjusted for multiple testing using the false discovery rate (FDR) correction method, controlling the FDR at 5%. Markers with FDR-adjusted *p*-values below 0.05 were considered significant and were visually highlighted in the selection coefficient plot. Red and blue circles denote significant selection against NN (t) and SS (s), respectively. When both t and s were significantly greater than zero, markers were interpreted as showing potential selection favoring the heterozygote (NS).

QTL Mapping

QTL analyses were conducted using the R/qtl and QTLtools packages (version 1.66; Broman *et al.*, 2003; version 1.3.1; Delaneau *et al.*, 2017) in R. QTL mapping was performed on the residuals extracted from models that accounted for positional effects. Additionally, the effect of variation in the chloroplast and mitochondrial genomes was assessed by including cross direction in the model alongside environmental effects. QTL mapping was conducted for 22 traits listed in Table 1. However, survival after flooding, being a binomial trait, lacked a sufficient number of F2 individuals for QTL mapping (Suppl. File 5).

For each trait, we used the *scantwo* function to perform a two-dimensional genome scan with a two-QTL model, applying the Haley-Knott regression algorithm (Haley & Knott, 1992). Penalties were calculated from 1,000 permutations of the *scantwo* function to support the stepwise fitting of multiple QTL models. The *stepwiseqtl* function was then employed, with a maximum of five QTL, using Haley-Knott regression to search for optimized models. We activated the *refine.locations* option in *stepwiseqtl* to improve the localization of QTLs and deactivated the *additive.only* option to allow for potential interactions between QTLs in the model.

332 We then looked into the summary output of *stepwiseqtl* to obtain information on the percentage
333 of variance explained by each QTL, as well as the peak LOD scores, and the additive (a) and
334 dominance (d) effects for each significant QTL, using allele N, identified in the best stepwise
335 models for each trait. For each identified QTL, we determined the 1.5 LOD confidence interval
336 using the *lodint* function in R/qtl. Finally, we used the *segmentsOnMap* function from QTLtools
337 to visualize QTL segments on the genetic map, and ggplot2 (version 3.5.1; Wickham, 2011)
338 to plot QTL effect sizes using the LOD scores obtained from the summary output of
339 *stepwiseqtl*. To assess the distribution of estimated additive and dominance effects, we
340 performed a separate Shapiro-Wilk normality test in R (Villasenor Alva & Estrada, 2009) for
341 each standardized effect type using standardized phenotype residuals derived from a GLM
342 that accounted for random effects, enabling comparisons across traits (Suppl. File 5). To
343 identify independent QTLs-those not associated with fertility QTLs or distortion regions-we first
344 excluded all QTLs located on chromosomes 4 and 7. Among the remaining QTLs, we removed
345 those whose genomic intervals overlapped with Fertility Score trait QTLs on the same
346 chromosome. Overlap was defined as any intersection between the start and end positions of
347 the QTL intervals.

348 **Analysis of Whole Genome Re-sequencing Data**

349 We used previously published resequencing data for 37 *A. nemorensis* and *A. sagittata*
350 individuals (Dittberner *et al.*, 2022). Additionally, we processed one *A. androsacea* individual
351 used as an outgroup (Dittberner *et al.*, 2022).

352 Reads were mapped to the new version of the *A. nemorensis* reference genome (see Genome
353 Assembly and Annotation) using BWA mem (version 0.7.17; Li & Durbin, 2009) and default
354 parameters. Read depth and other relevant read alignment quality control metrics were
355 computed using QualiMap v.2.2.1 (Okonechnikov *et al.*, 2016). Average read depth across all
356 37 samples was 23x. Variant calling was performed using GATK version 3.8 (McKenna *et al.*,
357 2010) and duplicates were marked using PicardTools. Filtering was based on quality
358 thresholds (DP<20; QD<2; MQ < 42; FS>60; SOR > 4; ReadPosRankSum < -6; MQRankSum
359 < -10.5). SNPs were required to be biallelic, and sites at which more than 30% of samples
360 were heterozygous and more than 20% missing were discarded. We polarized *A. nemorensis*
361 and *A. sagittata* individuals with a custom Python script using *A. androsacea* as an outgroup.
362 We performed phasing using the program shapeit2 (Delaneau *et al.*, 2014), assuming a
363 generation time of 1 year and mutation rate per generation of 7×10^{-9} and recombination rates
364 based on the genetic map described below. From these steps, our dataset resulted in
365 12,868,614 SNPs before filtering, from which we extracted 4,455,806. While curating the
366 assembly we discovered that segments on chromosomes 3, 4, 6, and 7 were inverted relative

367 to the genetic map. Rather than remapping the reads, we lifted over the VCFs themselves: for
368 every variant falling inside an inverted block, we mirrored its coordinate (new = start + end –
369 old) and reverse-complemented the REF and ALT alleles. The corrected VCF files were used
370 for all downstream analyses.

371 **Genome-wide Selection Scans**

372 Using the 37 full genome samples, we identified selective sweeps using biallelic SNPs and
373 the OmegaPlus software (Alachiotis *et al.*, 2012). The OmegaPlus statistics (omega) were
374 calculated using a grid size of 200,000 bp. We defined a minimum window size (minwin) of 50
375 kb and a maximum window size (maxwin) of 100 kb for computing LD values between SNPs.
376 Outlier omega statistics, which indicated selective sweeps had occurred, were determined
377 based on the genome-wide distribution of values. To minimize false positives arising from
378 demographic processes, the cut-off values for the omega statistics were established using
379 forward simulations in SLiM4 (Haller *et al.,* 2019; Haller & Messer, 2023) that were simulated
380 under the demographic history inferred by Dittberner *et al.* (2022). In short, the demography
381 consists of two pulses of interspecific gene flow between both species, one ancient pulse that
382 occurred directly after the species split and one recent migration event that occurred only
383 between the sympatric populations.

384 We generated 10,000 neutral datasets of 2 Mb each under the demographic history of ancient
385 and recent migration events that occurred between the two species, assuming a fixed
386 recombination rate for each simulated block (5.5e-8). The maximum omega value from each
387 simulated dataset was extracted, yielding a distribution of 10,000 maximum values. The 99th
388 percentile of this distribution that was used as the threshold to identify outlier windows
389 indicated selective sweeps had occurred.

390 To optimize sweep detection, we tested multiple combinations of grid, minwin, and maxwin
391 parameters (from 50 kb to 200 kb for grid size, and 50 kb to 100 kb for minwin and maxwin).
392 We then applied the optimized parameters to the real dataset of *A. nemorensis* and *A.*
393 *sagittata,* extracting only the sweep regions that exceeded the simulation-based threshold,
394 which were considered high-confidence selective sweep regions.

395 We further investigated the potential association between selective sweeps and phenotypic
396 traits by analyzing the overlap between the identified sweep regions and QTLs in *A.*
397 *nemorensis* and *A. sagittate* (Suppl. File 7). We used only high-confidence selective sweeps
398 in 200kb windows across the genome and overlaid these with the positions of all QTLs. We
399 focused on the 10 percent quantile regions around the QTL peak positions to increase
400 specificity.

401 **Fine-mapping the Largest QTL**

402 To fine-map the largest QTL, which was associated with Days to Flowering trait (first QTL on
403 chromosome 8), we identified F2 lines that were heterozygous for the QTL of interest and
404 homozygous for other Days to Flowering QTLs; a total of 15 lines resulted (Tables S3-4). We
405 sowed 90 F3 seeds per line (3 seeds per pot) in trays and transferred these to the cold
406 chamber for vernalization. After two weeks, we transplanted 1 seedling into each 7x7 cm pot
407 filled with *Topferde* (Einheitserde, Sinntal-Altengronau, Germany), resulting in 30 seedlings
408 per line. Pots were kept in the greenhouse for six weeks, after which plants were transplanted
409 into larger 9x9cm pots and moved to cold frames in the garden for seven weeks. During this
410 period, leaf material was harvested from each plant, and DNA was extracted from fresh leaves
411 using the NucleoSpin® 8 Plant II protocol. Subsequently, the plants were transplanted into
412 new 11x11 cm pots and placed on tables in the garden under a bird-protected cage. We
413 recorded flowering time, inflorescence height, internode length, number of shoots, plant
414 height, stem leaf density, stem height, and rosette diameter. Two successive trials were
415 carried out on 483 plants, the first started on 26.09.2022, the second on 16.11.2022. Plants
416 flowered between April and June 2023.

417 Geneious Prime® (version 2024.0.5) was used to design multiple species-specific primers
418 targeting the QTL region based on the *A. nemorensis* and *A. sagittata* genomes. We designed
419 five pairs of PCR markers, which divided the QTL region into four intervals. PCR was
420 conducted on the DNA of 407 plants to identify recombinants and locate their recombination
421 events within the predefined intervals. We built a quantitative model using the *glm* function
422 from the stats package (version 3.6.2) in R, accounting for both family and trial effects as fixed
423 factors (glm(flowering_time ~ family * (exp/tray_garden), family = quasipoisson). Then we
424 extracted residuals and ran another model on the residuals (glm(res_ftime ~ interval1 +
425 interval2 + interval3 + interval4, family = gaussian)). The model was run for each interval, with
426 the interval that best explained variation in flowering time residuals containing the flowering
427 time QTL (Suppl. File 6). The same procedure was then applied to assess the impact of each
428 interval on traits with overlapping QTLs in the same region as the F2 mapping population
429 (Inflorescence Height, Rosette Diameter, and Stem Height). Parental DNA and nuclease-free
430 water were used as positive and negative controls, respectively.

431 **Results**

432 **Phenotypic Differences of Ecologically Relevant Traits**

433 In total, 1,193 individuals germinated in the greenhouse and were set to grow in a common
434 garden situated at the University of Cologne. All replicates of *A. nemorensis* and *A. sagittata*

435 survived the common garden experiment (35 *A. nemorensis* and 35 *A. sagittata*). *A.*
436 *nemorensis* flowered approximately 12 days earlier than A. sagittate, (p<0.001, Table 1).
437 Mean values for 19 of the 22 scored traits differed between species (Table 1, Suppl. File 1,
438 Table 1).

439 **Table 1. Differences in phenotypic traits between parents**. This table summarizes the
440 phenotypic traits measured in the common garden experiment for F2 hybrids and their parental
441 replicates (*A. nemorensis* and *A. sagittata*). Means represent the average value for each trait
442 within parental replicates (35 individuals per species). "Distance" shows the absolute
443 difference between the species' means. The *p*-values indicate the significance of the
444 difference between species based on t-statistics.

Trait	**Mean *A. nem***	**Mean *A. sag***	**Distance**	***p*-value**
Days to Bolting (B.T)	157.2857	169.2857	12	1.302E-19
Days to Flowering (F.T)	183.5714	193.4286	9.8571	5.556E-14
Fertility Score (W.S)	0.0298	0.0295	0.0004	>0.63
Inflorescence Height (P.H)	35.2500	34.5714	0.6786	4.537E-02
Lamina Length (Lam)	1.2729	1.4646	0.1916	1.179E-03
Lamina L/W (LLW)	1.4760	1.7938	0.3178	3.702E-12
Leaf Length (L.L)	1.5562	1.7161	0.1599	>0.75
Leaf Width (L.W)	0.8589	0.8213	0.0376	1.667E-02
Number of Stem Leaves (N.L)	28.1429	18.1429	10	4.567E-20
Petal Length (Pet)	4.0569	5.3579	1.3010	1.887E-21
Petiole Length (Pti)	0.2833	0.2516	0.0317	1.084E-06
Rosette Diameter 1 (RD1)	1.8331	2.2419	0.4087	>0.23
Rosette Diameter 2 (RD2)	3.2946	3.6893	0.3947	4.922E-03
Rosette Diameter 3 (RD3)	3.3611	3.4424	0.0813	1.502E-03
Rosette Diameter 4 (RD4)	3.8805	3.9110	0.0305	7.447E-03
Side Shoots (Ssh)	2.7857	2.1429	0.6429	2.802E-02
Stem Height (S.H)	40.4286	34.4286	6	2.668E-09
Stem Leaf Density (SLD)	0.6979	0.5271	0.1707	5.508E-16
Stem Leaf Length (SLL)	2.3894	2.7921	0.4028	1.684E-04
Stem Leaf Width (SLW)	1.4021	1.2337	0.1684	2.966E-03
Petiole L/Lamina L (P.L)	0.2464	0.1886	0.0579	5.248E-07
Ground Shoots (Gsh)	0.2143	1.2857	1.0714	1.414E-08

445

446 *A. nemorensis* individuals displayed a markedly higher number of stem leaves compared to
447 *A. sagittata* (mean difference = 10 leaves, $p<0.001$), as expected for a trait that is often used
448 to determine the taxonomy of these species (Titz, 1979). The rosette diameter of the parental
449 genotypes differed significantly after 2, 3 and 4 weeks of growth (maximum $p<0.007$).
450 Moreover, trait variance among F2 hybrids was generally larger than trait variance between
451 their parental genotypes, suggesting transgressive segregation (Fig. 1). Although the seed
452 production of parents did not differ significantly (Fertility Score or W.S, $p>0.63$), the low fertility
453 observed for most F2 contrasted with the normal fertility of F1s (Fig. S1) and indicated
454 outbreeding depression (Fig. 1).

455 After four weeks of flooding, the survival rates of parental genotypes showed no significant
456 differences ($\chi^2(1,N=14)=0.43$, $p=0.5116$).

457 The cross direction impacted several traits, suggesting maternal influence and potential
458 cytoplasmic effects (Table S1). Traits such as Stem Leaf Length (SLL, $p=3.10^{-5}$), Rosette
459 Diameter at early stages (RD1, $p=8.10^{-5}$), and Petiole Length (Pti, $p=0.006$) exhibited strong
460 associations with the direction of the cross. Additionally, Petiole Length-to-Lamina Length
461 Ratio (P.L, $p=0.011$), Rosette Diameter 2 (RD2, $p=0.013$), and Rosette Diameter 3 (RD3,
462 $p=0.03$) also displayed significant maternal effects. *A. sagittata* maternal cytoplasmic
463 inheritance decreased rosette lamina size on the rosette, but increased it on the stem (Table
464 S1, Fig. S2). In contrast, the majority of traits, including Days to Bolting (B.T), Days to
465 Flowering (F.T), Fertility Score (Seed Production or W.S), and structural traits like
466 Inflorescence Height (P.H) and Number of Stem Leaves (N.L), showed no cytotype effects
467 ($p>0.05$), indicating limited or negligible maternal influence.

468 Spearman correlation analysis of 22 traits in the F2 population revealed relationships among
469 traits (Figs. S3-4). Traits associated with leaf shape, such as Lamina Length (Lam) and Leaf
470 Width (L.W), exhibited strong positive correlations ($r > 0.8$, $p < 0.001$). Similarly, Rosette
471 Diameter (RD1–RD4) measured at different time points showed strong positive correlations (r
472 > 0.7, $p < 0.001$).

473 Developmental traits, such as Days to Bolting (B.T) and Days to Flowering (F.T), showed
474 moderate correlations with vertical growth traits, including Stem Height (S.H) and
475 Inflorescence Height (P.H). For instance, Inflorescence Height was positively correlated with
476 Days to Flowering ($r = 0.535$, $p < 0.001$), suggesting that later-flowering individuals allocate
477 more resources to vertical growth. In contrast, Fertility Score (Seed Production or W.S), a

478 component of fitness, exhibited weaker and often insignificant correlations with other traits,
479 indicating potential independence from vegetative and structural phenotypes.

480 Petiole traits, including Petiole Length (Pti) and its ratio to Lamina Length (P.L), which are
481 often associated with shade avoidance strategies, were moderately correlated with rosette
482 size and leaf shape traits such as Leaf Width (L.W). Overall, these findings highlight the
483 interdependencies among structural traits (e.g., plant size, leaf shape), developmental traits
484 (e.g., flowering time, rosette size over time), and fitness components in *Arabis* F2 hybrids. The
485 statistical analyses of ecologically relevant traits in the common garden experiment provide
486 valuable insights into the extent of phenotypic integration and the nature of resource allocation
487 strategies in the F2 hybrid population.

488

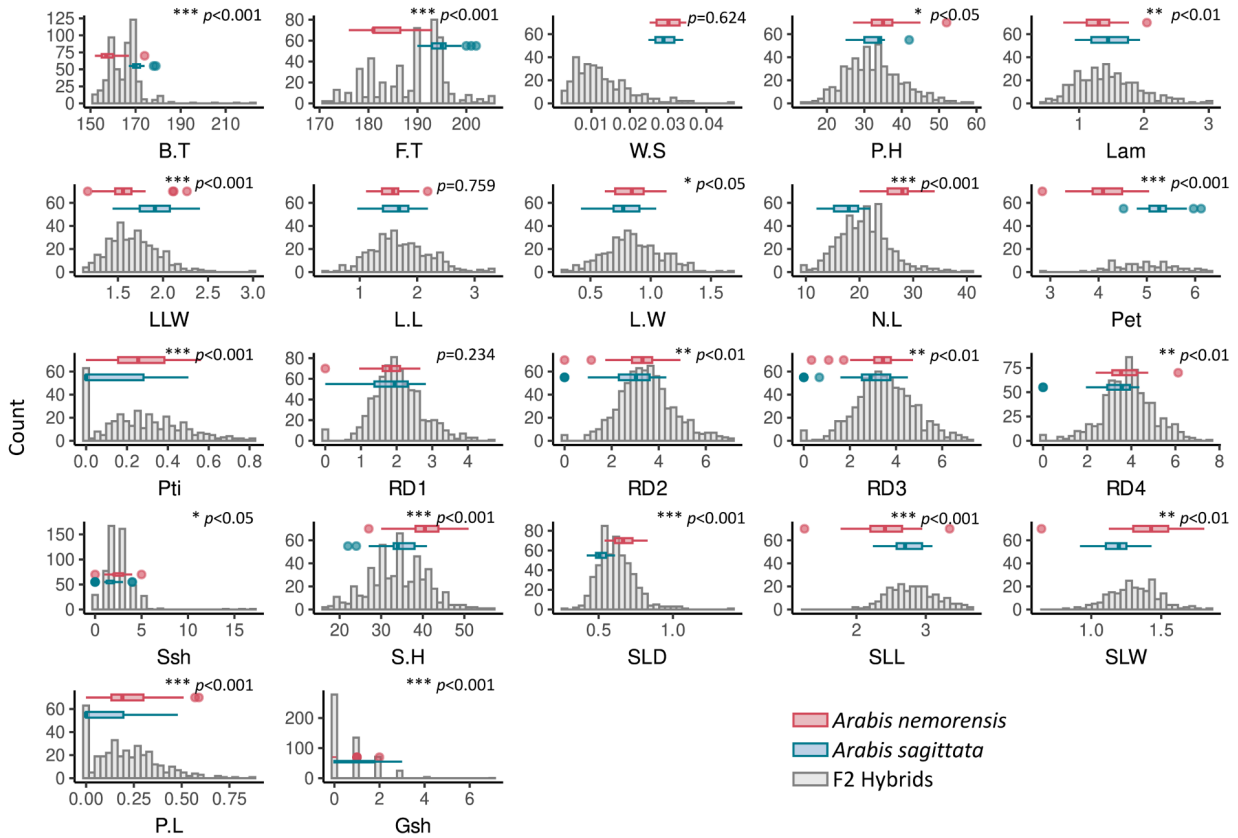

489 **Figure 1. Phenotype distribution in the F2 progeny and their parental lines.** Histograms
490 illustrate the distribution of traits in the 1,193 plants of the F2 generation grown in common
491 garden. Boxplots highlight trait variations between the two parental lines and indications of
492 transgressive segregation in their offspring. The *p*-values and stars depict the significance of
493 trait differences between parents * p<0.05, ** p<0.01, *** p<0.001. Abbreviations are as
494 follows: Days to Bolting (B.T), Days to Flowering (F.T), Fertility Score - Seed Production (W.S),

495 Inflorescence Height (P.H), Lamina Length (Lam), Lamina Length-to-Width Ratio (LLW), Leaf
496 Length (L.L), Leaf Width (L.W), Number of Stem Leaves (N.L), Petal Length (Pet), Petiole
497 Length (Pti), Rosette Diameter at four time points (RD1-4), Side Shoots (Ssh), Stem Height
498 (S.H), Stem Leaf Density (SLD), Stem Leaf Length (SLL), Stem Leaf Width (SLW), Petiole
499 Length-to-Lamina Length Ratio (P.L), and Ground Shoots (Gsh).

500 **Genetic Map, Pre- and Post-zygotic Selection Distortion**

501 To investigate the genetic architecture underlying trait variation, we used a reduced
502 sequencing approach to determine the genotypes of 742 F2 individuals at 2,082 reliable SNP
503 markers with the help of high-quality genome assembly (Fig. S5, Suppl. File 2, Table 1), and
504 constructed a genetic map. The map consisted of eight linkage groups (LGs), which were
505 numbered according to the chromosome numbers of *Arabis alpina*. The length of the linkage
506 map was 240 cM, with 160 to 369 markers per chromosome (Table S2). Contrasting the
507 genetic and physical distances of SNPs along chromosomes showed that recombination was
508 higher on chromosome arms compared to in centromeric regions (Figs. S6-7).

509 The analysis of allele and genotype frequencies along the genome uncovered strong
510 segregation distortions in the F2 population. A strong segregation distortion was found on
511 chromosomes 4 and 7 with the percentage of N alleles dropping from 50% (expected) to 32%
512 (Fig. 2A). Because the sequencing data was mapped on the high-quality *A. nemorensis*
513 genome, we can conclude that this depletion is clearly not due to mapping biases. To
514 disentangle prezygotic from postzygotic mechanisms of allele distortion, we estimated the
515 difference between expected and observed genotype distributions across the genome using
516 a chi-square test (Fig. 2B), and inferred selection coefficients against each type of
517 homozygote. This analysis showed that the segregation distortions on chromosome 7 and on
518 the tip of chromosome 4 were not due to postzygotic selection on the genotype. Yet, it
519 identified 6 regions in the genome with a significant excess of heterozygotes, three of which
520 were particularly strong on chromosomes 1 and 8. It further highlighted one region in
521 chromosome 3 with massively depleted homozygotes.

522 The extent of segregation distortion found throughout the genome appeared to be mostly due
523 to interactions between local alleles. For example, no genetic association was observed
524 between the distortion on chromosomes 4 and 7 (Fig. S8). Nevertheless, we find biased
525 transmissions of parental alleles on chromosomes 2 and 5, as well as chromosomes 3 and 8
526 (Fig. S8).

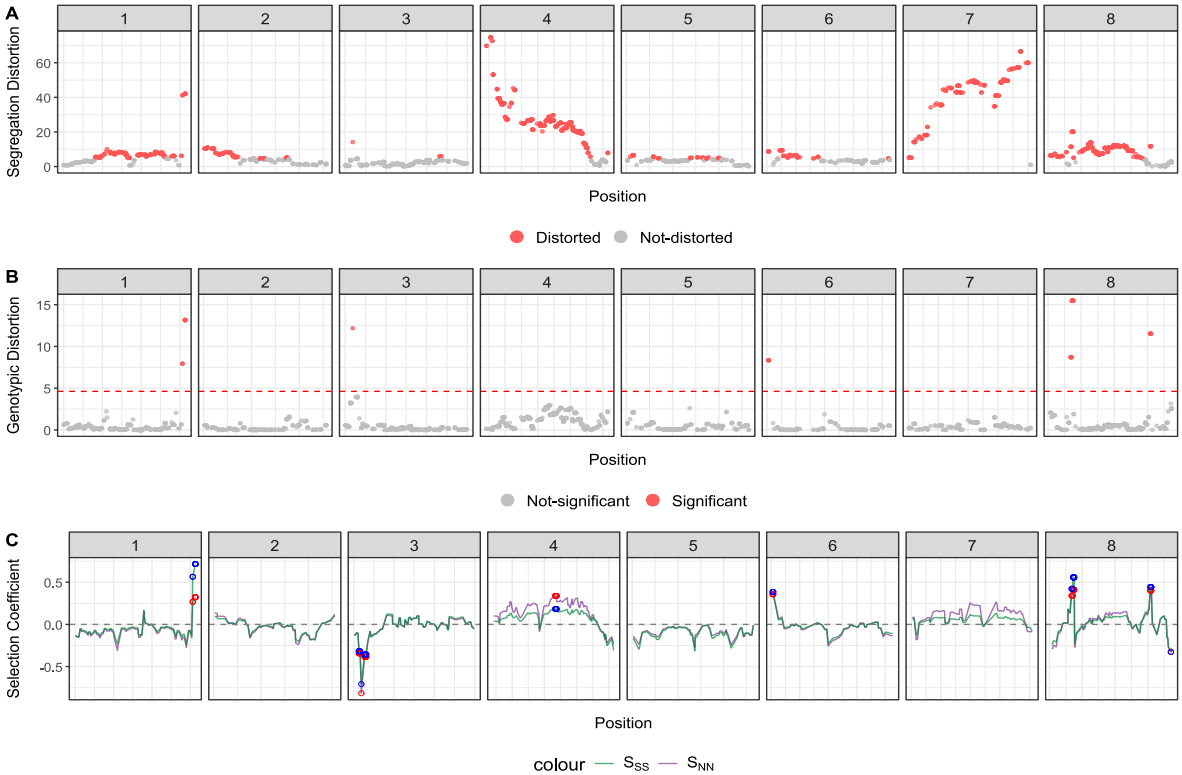

527

528 **Figure 2. Segregation distortion, genotypic distortion and strength of selection along**
529 **the genome.** This figure illustrates segregation distortion, genotypic distortion, and the
530 strength of selection across the genome in the F2 population. The x-axis represents marker
531 positions along the genome across the eight chromosomes (2082 markers). The y-axis in (A)
532 and (B) shows $-\log_{10}(p\text{-value})$; the y-axis in (C) represents the selection coefficient. (A)
533 Gametic distortion: shown by the deviation of SNPs from expected Mendelian segregation
534 ratios, assessed using a segregation distortion test (profileMark) with Bonferroni correction for
535 multiple testing (threshold $p < 2.4 \times 10^{-5}$). Significant deviations are highlighted in red. 1,257
536 markers are significantly distorted. (B) Genotypic distortion: calculated as the deviation of
537 observed genotypes from expected values according to the HWE, assessed using a chi-
538 square test. Bonferroni-adjusted significant differences are highlighted in red. Only 47 markers
539 surpassed the Bonferroni significance threshold. (C) Selection coefficient (s): calculated based
540 on deviations from expected allele frequencies, with selection on allele S represented in green
541 and on allele N in purple. Red and blue circles indicate markers where genotype frequencies
542 significantly deviate from the HWE (FDR-adjusted $p < 0.05$, chi-squared test), suggesting
543 selection at those loci. Red circles represent significant selection against the NN genotype (t);
544 blue circles represent selection against the SS genotype (s). Loci where both t and s are
545 significant and positive, indicate potential selection favoring the heterozygote (NS).

546

547 **Genetic Architecture of Ecologically Relevant Traits**

548 We detected significant QTLs for 20 of the 22 traits we scored (Table 2). The number of QTLs
549 per trait ranged from 1 (Lamina Length) to 5 (Days to Flowering). The most significant QTL
550 (LOD score > 40) was identified on chromosome 8, accounting for more than 20% of the
551 variation in flowering time. In contrast, the lowest LOD score (3.027) was observed in one of
552 the Leaf Width QTLs. In total, 58 QTLs were identified along the genome (Table 2). We
553 observed overlapping QTLs for multiple traits, including 9 on chromosome 1; 3 on
554 chromosome 2; 11 on chromosome 3; 4 on chromosome 4; 3 on chromosome 5; 2 on
555 chromosome 6; 6 on chromosome 7; and 20 on chromosome 8 (Fig. 3). Notably, one QTL
556 associated with the Fertility Score on chromosome 6 did not overlap with any other QTLs (Fig.
557 3, Table 2)

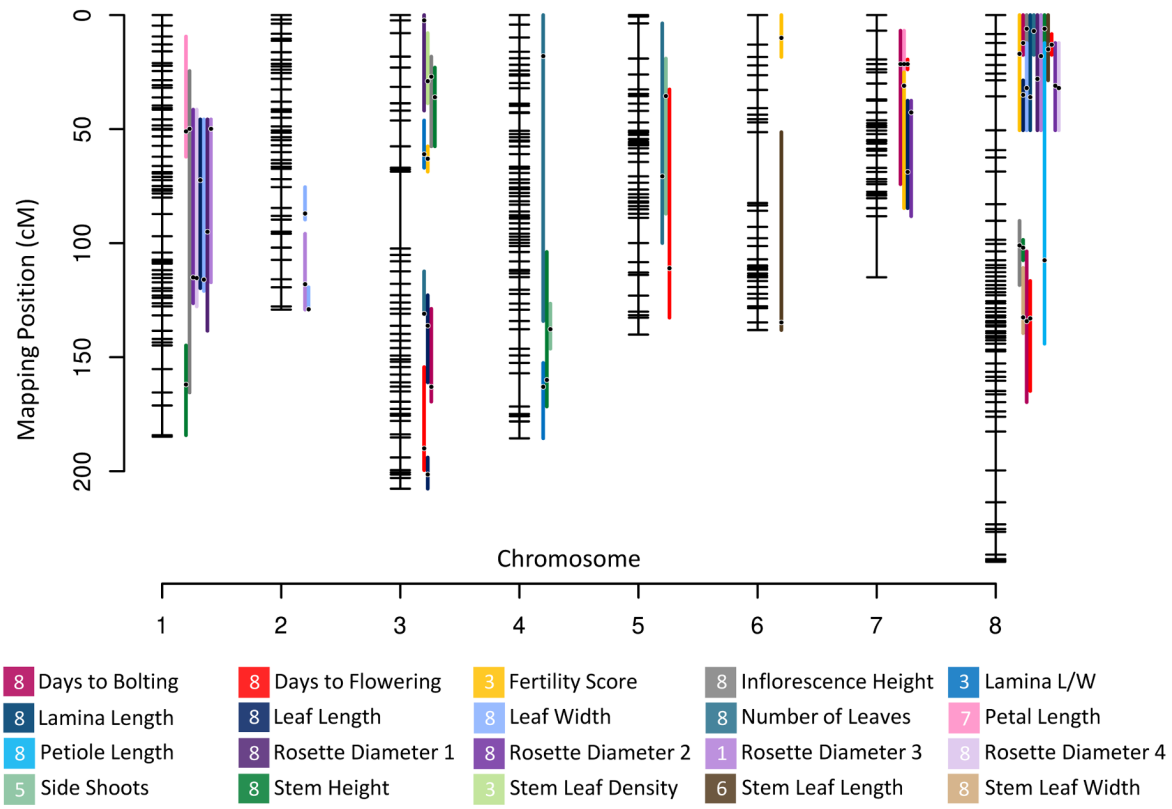

558

559 **Figure 3. Genetic map with QTLs for ecologically relevant traits.** The plot above illustrates
560 significant QTLs that were detected and located on the genetic map. Horizontal bars represent
561 mapped SNP markers. Gaps between bars stand for the genetic distance between SNP
562 markers in cM (centimorgan). Traits are listed in alphabetical order. The chromosome
563 containing the strongest QTL of each trait appears in the square.

564

565 The strongest QTLs for traits such as Days to Bolting, Days to Flowering, Inflorescence Height,
566 Leaf Length and Width, Number of Stem Leaves, and Rosette Diameter after 1, 2, and 4
567 weeks, as well as Stem Height and Stem Leaf Width, were all located on chromosome 8.
568 Additionally, strongest QTLs for Petal Length, Rosette Diameter 3, Side Shoots, Stem Leaf
569 Density, and Stem Leaf Length were identified on chromosomes 7, 1, 5, 3, and 6, respectively.
570 For all traits, the additive effect of the *A. nemorensis* allele was either positive or negative,
571 confirming that transgressive genetic variation can arise in most traits in this selfing species
572 by fixing a new combination of alleles (Table 2).

573 The distribution of fertility scores, which was measured as the weight of seeds contained in
574 10 siliques, indicated that F2 individuals tended to be less fertile than the parental lineages.
575 The genetic architecture of fertility score variation was dominated by a large-effect QTL (LOD
576 = 8.774) on chromosome 3 (Fig. S9), which explained more than 30% of the phenotypic
577 variation and involved inter-allelic incompatibility at position 8,362,080 bp on chromosome 3
578 (QTL interval: 6,744,303 to 9,601,991 bp, Fig. S9). Individuals with the NS heterozygous
579 genotype at this marker displayed markedly lower fertility. In addition, three smaller QTLs
580 explaining 2.683%, 4.641%, and 3.507% of the variation were found on chromosomes 6, 7,
581 and 8, respectively. It can be concluded that the genetic basis of outbreeding depression is
582 relatively simple in this population.

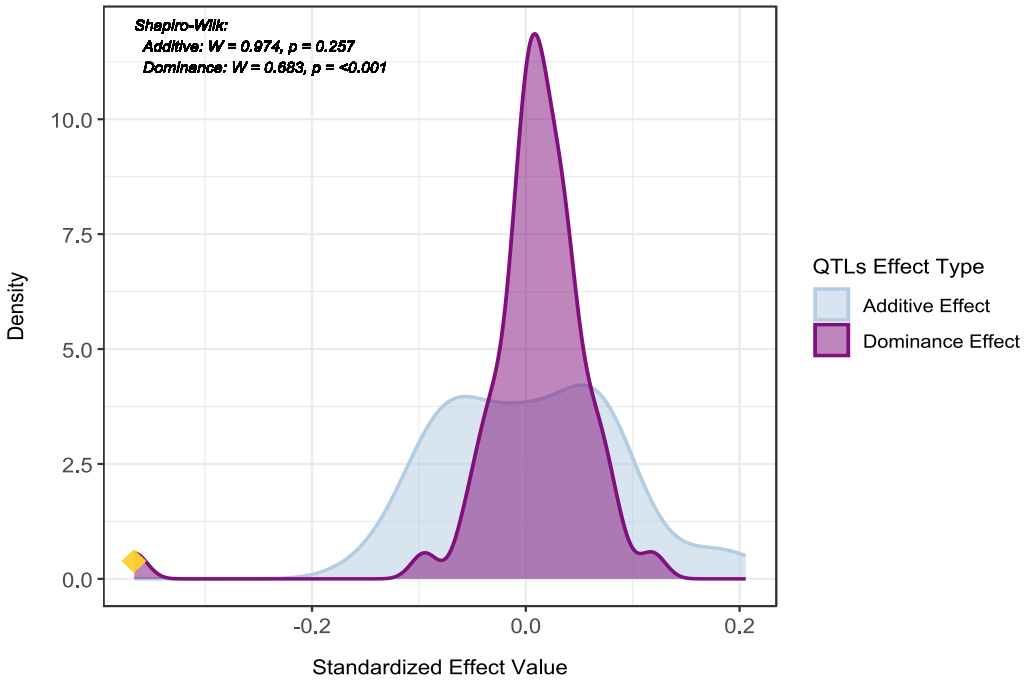

583

584 **Figure 4. Distribution of standardized QTL estimated additive and dominance effects.**
585 The figure above displays the distribution of standardized estimated additive and dominance
586 effects for QTLs associated with ecologically relevant traits identified in the F2 population.

Each curve represents the density of standardized effect sizes for a distinct type of genetic effect: additive effects (in light blue) and dominance effects (in purple). The yellow diamond marks the dominance effect of the strongest QTL for Fertility Score (W.S) on chromosome 3. Effect values were estimated using interval mapping on standardized phenotype residuals derived from a GLM that accounted for random effects, enabling comparisons across traits. Density distributions illustrate the range and frequency of QTL contributions. Additive effects showed a Gaussian distribution (Shapiro-Wilk: W = 0.974, p = 0.257), whereas dominance effects approximated a logistic distribution after excluding the outlier dominance effect of a QTL on chromosome 3 (Shapiro-Wilk: W = 0.683, $p < 0.001$).

Of the 22 traits scored, Ground Shoots (Gsh), Petiole Length-to-Lamina Length ratio (P.L), and Survival to Flooding revealed no significant QTL. For two of these three traits (Ground Shoots, Petiole Length-to-Lamina Length ratio), significant differences between species were observed. The absence of QTLs for these traits suggests they may have a polygenic genetic basis, and the effect of individual variants may be too small to be detected.

We conclude that the two parental lineages differ genetically in many traits, with size effects of various sizes. The number of detected QTLs allows us to describe the size effects of genetic variation that can be generated by hybridization in this system. The standardized additive effects were normally distributed (Shapiro-Wilk: W = 0.9744, p = 0.2573, Fig. 4), ranging from a minimum of -0.15 to a maximum of 0.20 with a median of 0.008 (mean = 0.005, s.d.= 0.08, skewness = 0.29, kurtosis = 2.6). QTLs with the largest effect controlled flowering time, stem height, inflorescence height, leaf number and lamina shape contributing to the heavy tail of the distribution of additive effect (Figs. 4, S10). Standardized dominance effects instead approximated a logistic distribution (Shapiro-Wilk: W = 0.683, $p < 0.001$), ranging from -0.36 to 0.11 with a median of 0.012 (mean = 0.008, s.d. = 0.062, skewness =-3.70, kurtosis = 23.5). The dominance effect of the fertility score QTL on chromosome 3 was an outlier to this distribution (Fig. 4).

618 **Table 2. QTLs of ecologically relevant traits in the *Arabis* mapping population.** This table
619 summarizes the number, chromosomes, peak positions, LOD scores, percentages of
620 phenotypic variance explained, and estimated additive and dominance effects of allele S for
621 each QTL. The number of observations per trait in the F2 population is indicated. Significance
622 differences between parental lines are denoted as follows: *** ($p < 0.001$), ** ($0.001 < p <$
623 0.01), * ($0.01 < p < 0.05$), . ($0.05 < p < 0.1$) (details in Suppl. File 5)

Trait	No. of Observations	Significance ofParental Differences	Chr	Position (bp)	Position (cM)	LOD	%Variance Explained	est *a*	est *d*
Days to Bolting (B.T)	631	***	3	20040893	163	5.146	3.130	0.005914	-0.012765
			7	1835566	21.5	5.359	3.263	0.010990	0.002648
			8	2061023	12.2	7.786	4.783	-0.011989	0.000447
			8	19500950	134.2	12.396	7.746	0.016244	-0.003620
Days to Flowering (F.T)	578	***	3	26882840	190	9.915	4.785	0.012242	-0.001815
			5	23418119	111	4.868	2.289	-0.007092	0.003427
			7	1835566	21.5	11.241	5.423	0.011243	-0.001854
			8	2061023	13	42.112	23.075	-0.021252	0.008320
			8	18832553	133	9.374	4.488	0.009159	-0.005437
Fertility Score (W.S)	552		3	8362080	63	8.774	6.165	-0.056270	-0.366350
			6	1052484	10	3.897	2.683	0.172390	-0.055580
			7	3192272	31	6.663	4.641	0.205690	-0.053080
			8	3118527	17	5.070	3.507	0.178080	-0.028820
Inflorescence Height (P.H)	578	.	1	9004320	49.9	4.166	2.385	-0.012682	0.062053
			3	2664384	27	11.394	6.714	0.078301	0.016361
			8	1180103	6	20.789	12.728	-0.094477	0.076771
			8	10128705	101	6.383	3.686	-0.062798	-0.038649
Lamina Length (Lam)	436	*	8	5481058	36.0	4.334	4.475	-0.075590	0.042250
	436	***	3	6744303	61	15.635	14.890	0.089464	-0.031374

Trait	No. of Observations	Significance ofParental Differences	Chr	Position (bp)	Position (cM)	LOD	%Variance Explained	est *a*	est *d*
Lamina L/W (LLW)			4	38897287	163	4.045	3.620	0.041307	0.028487
Leaf Length (L.L)	436		1	13071968	72.4	4.458	3.766	0.071867	-0.012244
			3	14255522	136.2	5.214	4.423	-0.007829	0.118366
			3	29031007	201.4	5.617	4.775	0.066584	-0.094772
			7	14342773	68.8	4.284	3.615	-0.020747	0.086727
			8	5624776	35	9.433	8.183	-0.104748	0.036218
Leaf Width (L.W)	436		1	21722429	116	4.313	3.893	0.069770	0.045460
			2	19435694	87	3.027	2.713	-0.043950	0.056000
			2	25576894	129	5.987	5.452	0.091250	0.012400
			8	4356973	32	6.705	6.129	-0.081970	0.036770
Number of Stem Leaves (N.L)	625	***	3	14075550	130.9	4.581	2.557	0.025147	0.059693
			4	7558305	18	4.001	2.228	0.056356	0.010451
			5	16624270	70.7	5.384	3.014	-0.055649	0.004690
			8	1180103	7	28.109	17.139	-0.119377	0.052082
Petal Length (Pet)	106	***	1	9074627	51	4.863	15.820	0.064910	0.039080
			7	1835566	21.5	5.689	18.850	0.079160	0.013480
Petiole Length (Pti)	361	**	8	10723493	107.5	3.814	4.749	-0.153200	-0.035130
Rosette Diameter 1 (RD1)	695		1	17879753	95	4.498	2.747	0.068440	-0.020590
			3	623617	2.3	3.632	2.212	0.054350	0.023100
			8	4362085	28	6.942	4.275	-0.074250	0.032990
Rosette Diameter 2 (RD2)	700	.	1	21954996	115	6.158	3.703	0.079730	0.013670
			7	5769578	42.7	3.839	2.291	-0.056060	0.024000
			8	4356973	31	7.822	4.729	-0.085450	0.033910
	696	.	1	9004320	49.9	9.389	5.683	0.102710	-0.005208

Trait	No. of Observations	Significance ofParental Differences	Chr	Position (bp)	Position (cM)	LOD	%Variance Explained	est *a*	est *d*
Rosette Diameter 3 (RD3)			2	23541930	118	4.024	2.392	0.043216	0.071859
			8	2718077	18	7.209	4.332	-0.087105	0.022622
Rosette Diameter 4 (RD4)	701	*	1	21722429	115.3	4.330	2.678	0.061815	0.014845
			8	4356973	32	7.814	4.888	-0.078677	0.035138
Side Shoots (Ssh)	595	*	4	36501835	137.7	3.859	2.842	-0.119930	-0.038550
			5	5129643	35.5	4.875	3.605	0.126580	0.031450
Stem Height (S.H)	625	***	1	29847516	162	3.594	1.778	-0.029247	0.036282
			3	4035375	36	13.598	6.984	0.074366	0.005981
			4	38897287	160	4.386	2.177	0.042699	-0.004189
			8	1180103	6	26.851	14.500	-0.091994	0.070533
			8	10506892	102	7.858	3.951	-0.059677	-0.004408
Stem Leaf Density (SLD)	624	***	3	3491752	29	5.760	4.162	-0.052426	-0.018081
Stem Leaf Length (SLL)	259	**	6	21070306	134.8	5.918	9.356	0.046349	0.011155
			8	3118527	15	3.967	6.163	-0.035380	0.011240
Stem Leaf Width (SLW)	259	***	8	18832576	132.5	13.228	20.958	-0.084603	0.017725

Genes Responsible for Flowering Time

The largest QTL detected in this study impacts the timing of flowering and is located on chromosome 8, where two well-known genes that control flowering time are found: *FLC*, a regulator involved in the vernalization pathway, and *CONSTANS*, a regulator involved in the photoperiod pathway (Andrés & Coupland, 2012). *FLC* has been shown to be a key variant shaping flowering time in many Brassicaceae species, including the congeneric species *Arabis alpina* (Albani *et al.*, 2012). The gene *CONSTANS* is also located within the boundaries of this QTL. In order to test whether one of these candidate genes was responsible for the variation, we selected 15 F2 individuals that were heterozygous in the QTL region of chromosome 8 and homozygous on the other QTLs, and we grew 30 of their seeds. A total of

410 plants were assessed for flowering time in 15 F3 families and two trials (Fig. S11, Tables S3-4).

With 410 plants and a QTL region that was ~17 cM, we expected 80 recombinants. Interestingly, we identified 138 recombinants, suggesting that the recombination rate had been slightly underestimated in the F2 population. We compared four models to identify the chromosomal fragments that best explained variation in flowering time, after accounting for all other factors of the experimental design. Using Akaike's criterion and comparing *p*-values, we identified fragment 2 as the most likely to contain the variants causing a difference in flowering time (Fig. 5, p=0.0118). This segment ranges from position 1,831,324 bp to position 2,125,083 bp at the beginning of chromosome 8. Although this ~300 kb region does not contain *FLC* or *CO*, it contains 64 other genes, 31 of which have a known ortholog in *Arabidopsis thaliana*. Only 1 of these, *TFL1*, is known to regulate flowering time in *A. thaliana* and *A. alpina*, with a loss of function inducing early flowering in both species (Cerise *et al.*, 2023). *A. sagittata TFL1* differs from the *A. nemorensis* copy by 2 amino acid exchanges: Asparagine 3 is changed to Isoleucine and Serine 50 is changed Tyrosine. The *A. nemorensis* version at both sites is conserved in most Brassicaceae, like *A. thaliana*, where *TFL1* function has been experimentally verified (Andrés & Coupland, 2012). Nevertheless, both positions are not strictly conserved.

In contrast to most *TFL1* genes from the Brassicales, several species within (*Capsella rubella*, *Sinapis alba*) and outside of this group are missing the start codon and protein translation starts at the conserved Methionine codon at position 4. At position 50, Serine is the most common amino acid not only in the Brassicales group, but also in other plant groups, but other amino acids (Alanine, Threonine, Phenylalanine) are found in other Brassicaceae *TFL*1 sequences. Because *A. sagittata* carries derived amino acids at two moderately conserved positions, gene activity may be decreased compared to the more ancestral *A. nemorensis* allele. Fine-mapping, however, allowed us to exclude the role of flowering loci such as *FLC* or *CO* that locate on the same chromosome arm of chromosome 8.

Although there were QTLs for Inflorescence Height, Rosette Diameter, and Stem Height, on chromosome 8 in F2s, the chromosomal region that was fine mapped did not explain the variation of these traits in F3s. Inflorescence Height, Rosette Diameter and Stem Height are thus controlled by QTL(s) independent of the QTL for Flowering Time in the *TFL1*-containing fragment, with the S allele advancing flowering compared to the N allele.

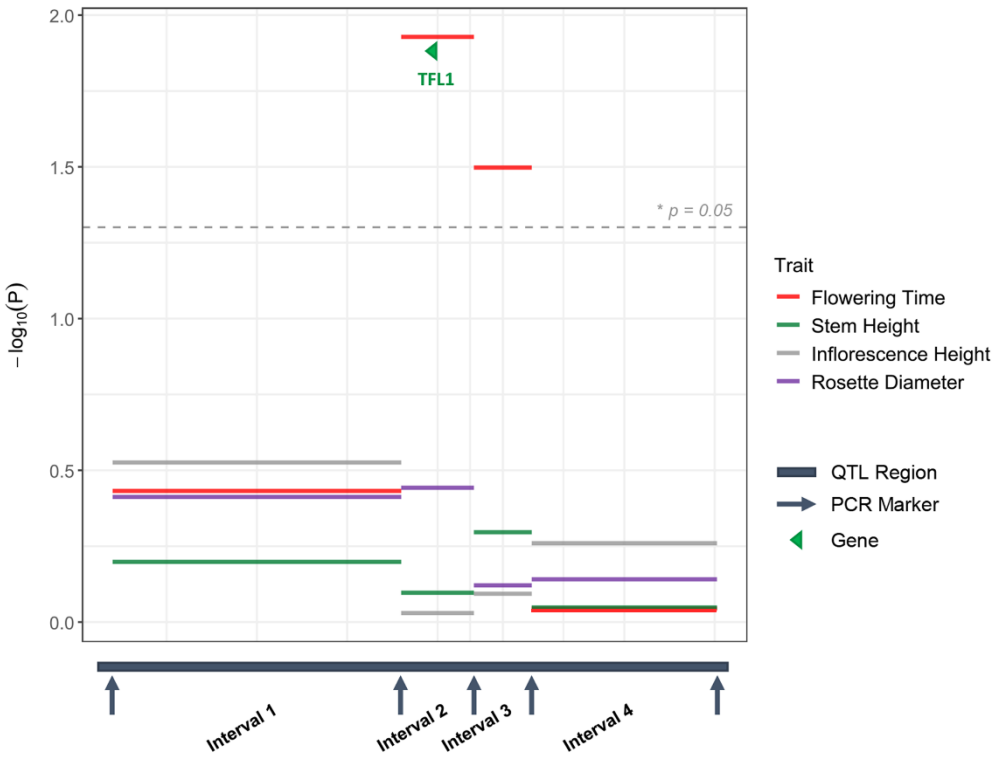

667

668 **Figure 5. Association between 4 DNA fragments and flowering time within 15 F3 families**
669 **segregated for the chr8 flowering time QTL.** The figure illustrates the role of genomic
670 intervals within the QTL region in explaining variations in Flowering Time, Inflorescence
671 Height, Rosette Diameter, and Stem Height. The x-axis represents region of the strongest
672 Flowering Time QTL, divided into intervals defined by species-specific primers with adjusted
673 lengths for fine mapping. The dashed line indicates the significance threshold. Different bar
674 colors represent different traits. The *TFL1* gene was detected in interval 2, which shows the
675 strongest effect on flowering time.

676 **Overlap of Parental QTLs with the History of Selection in the Parental Lineages**

677 In order to test whether genetic differences between lineages were influenced by selection for
678 ecological specialization in the two parental lineages, prior to hybridization, we used previously
679 published population genomics data to determine regions with signature of selective sweeps
680 (Dittberner *et al.*, 2022). We detected 35 and 82 genome regions carrying signatures of
681 selective sweeps in *A. nemorensis* and *A.sagittata*, respectively, which prompted us to ask
682 whether variable traits were disproportionately targeted by natural selection in their lineage or
683 origin (Fig. S12). Many of the 58 QTL regions spanned large parts of chromosomes,
684 sometimes overlapping with multiple independent selective sweeps (Fig. S13). We tested

whether the distance between QTL peak and selective sweep was shorter than expected by a permutation test. QTL peaks did not tend to be located close to selective sweep signatures. We also did not detect significant overlaps between regions with distorted segregation and regions carrying selective sweeps (not shown). The genetic variation segregating in the F2 population thus does not appear to reflect the history of selection in the hybridizing lineages, yet some individual QTLs may reflect recent selection. For example, sweeps overlapped with 5 of the 7 genomic regions with QTLs for rosette size (Fig. S12). In contrast, no signature of a putative selective sweep was found in the *TFL1* region.

Discussion

Hybridization between species is pervasive in both past and contemporary ecosystems (Lewontin & Birch, 1966; Stull *et al.*, 2023). By bringing together alleles that contribute to different ecological specialization, it can facilitate the emergence of a new allelic combination that may surpass the performance of the parental genotypes and be fixed via selfing. Hybridization may therefore become pivotal in the rescue of endangered selfing species with very low levels of genetic diversity (Frankham, 2015). Here, we take advantage of a hybridization hotspot we identified previously to disentangle the genomic and ecological properties of genetic variation released after hybridization, some of these properties may propagate in the population via selfing. An F2 generation was obtained by crossing individuals representative of the two species in the sympatric population where they naturally hybridize (Dittberner *et al.*, 2019; Dittberner *et al.*, 2022).

The genetic analysis of allelic transmission in the F2 population first revealed the genomic barriers that skew allele segregation in hybrid offspring. Indeed, several regions of the genome displayed highly distorted transmission. For the two most strongly distorted regions on chromosomes 4 and 7, the genotypic composition of the F2 fits Mendelian expectations, suggesting that the distortion happens before fertilization, as a result of biased gamete formation. Both of these distortions drive the *A. sagittata* allele to high frequencies in the F2 offspring population. The predominance of one allele among mature gametes produced in a heterozygous individual represents a very strong evolutionary force called the meiotic drive (Sandler & Novitski, 1957; Pinkas *et al.*, 1985; Clarke *et al.*, 2004; Domínguez *et al.*, 2005). The meiotic drive can massively accelerate the fixation of alleles linked to the driver locus. Driver alleles may outcompete non-driver alleles during pollen tube growth in heterozygotic selfing plants, thereby biasing the paternal transmission of alleles in favor of the offspring (e.g., Snow & Spira, 1996; Aronen *et al.*, 2002; Lankinen *et al.*, 2009). In female gametes, any molecular change that favors allele transmission into the polar body would lead to preferential maternal transmission (Fishman & Kelly, 2015; Finseth *et al.*, 2015). Here, since genotype

720 frequencies fulfil the HWE, the driver alleles should outcompete the non-driver alleles in both
721 male and female gametogenesis (Malik, 2005). Many mechanisms can lead to gametic drive
722 in plants, because gametes undergo haploid cell division, a step that does not exist in animals
723 (Finseth, 2023). As a consequence, about 60% of plant genes are expressed in the haploid
724 phase (Chettoor *et al.*, 2014; Rutley & Twell, 2015; Klepikova *et al.*, 2016), and variants have
725 been identified in genes controlling cell division in gametes of *A. thaliana* (Parker *et al.*, 2025).

726 In addition to segregation distortion at the gametic level, we also detected regions in the
727 genome that experienced biased transmission as a result of the distorted frequency of
728 heterozygotes. One locus on chromosome 3, for example, was markedly depleted in
729 heterozygotes, despite equal transmission of the two alleles. This locus was close, but distinct
730 from a second locus that decreased the seed production of heterozygotes by 30%. This
731 pattern, which is also known as allelic underdominance, characterizes the genome of a pair of
732 alleles in *A. thaliana* (Smith *et al.*, 2011). The causal variant mapped to structural changes in
733 a tandem array of duplicated genes and altered kinase activity (Smith *et al.*, 2011). In selfing
734 species and their hybrids, underdominance will not pose a significant threat to the equal
735 transmission of alleles provided that F1 hybrids are viable – as is the case in this study
736 system– because half of the descendants of heterozygote individuals will return to
737 homozygosity.

738 Allelic underdominance is a form of Dobzhansky-Muller (DM) incompatibility (Dobzhansky,
739 1936; Muller, 1942). DM incompatibilities arise after alleles are fixed in the diverging parental
740 lineages without being naturally selected to function together. Interactions between alleles
741 segregating at different loci can also cause DM incompatibilities, but, interestingly, no
742 segregation distortions were detected in any major interlocus in this system, nor did any
743 interactive QTLs determine fertility. DM incompatibilities have been studied extensively in
744 many taxa (Bomblies & Weigel, 2007; Masly & Presgraves, 2007; White *et al.*, 2011; Schumer
745 *et al.*, 2014; Zuellig & Sweigart, 2018; Coughlan & Matute, 2020). Although such
746 incompatibilities are assumed to evolve completely neutrally, they can also result from local
747 adaptation (Alcázar *et al.*, 2014).

748 However, whereas only 2 loci showed underdominance, 6 loci showed selection for
749 heterozygote genotypes. This discrepancy indicates that in this system the compensation of
750 deleterious variants in heterozygote regions is more predominant than the emergence of DM
751 incompatibilities (Clo *et al.*, 2021). Indeed, 6 regions in the genome show an excess of
752 heterozygotes. This imbalance indicates that the low effective population sizes of the two
753 species, as well as their relatively recent origin, will have increased the fixation of deleterious
754 alleles faster than they will have fixed new incompatible mutations (Simons & Sella, 2016;

755 Dittberner *et al.*, 2022). As recombination and selfing will proceed in further generations after
756 hybridization, high-fitness individuals are expected to arise that will have purged these
757 variants. The interplay between purging and recombination has been shown to cause
758 heterogeneous rates of introgression along the genome of hybridizing taxa (Schumer *et al.*,
759 2018).

760 The pattern of past introgression in the *Arabis* system is in fact heterogeneous along the
761 genome (Dittberner *et al.*, 2022). Yet, our work shows that the selective removal of deleterious
762 variants is probably not the only force affecting this system today. The massive transmission
763 advantage of the *A. sagittata* alleles on chromosomes 4 and 7 implies that any allele that is
764 located close to the driver of the distortion will readily introgress into the local *A. nemorensis*
765 population, whether it is deleterious or ecologically relevant. Linked QTLs of small effect in the
766 vicinity of the distortion, however, will be hard to detect. Other approaches, such as, for
767 example, transcriptome analyses, are needed to determine the potential ecological relevance
768 of genetic variation hitchhiking with gametic driver alleles.

769 The genomics of allele transmission is clearly shaping the consequences of hybridization in
770 this system. Yet, segregation distortions, incompatibilities, and overdominance were
771 detectable on a limited number of loci. Due to their simple genetic basis, the loci are unlikely
772 to block genetic exchanges (Li *et al.*, 2022). The genetic architecture of the comprehensive
773 panel of traits quantifying growth rate, growth form, the transition to flowering, plant height and
774 the production of seeds allowed us to examine the extent to which gene flow at ecologically
775 relevant QTLs was hindered by genomic barriers in this system. Results demonstrated that
776 the parental lineages differ genetically in most traits, with about 48% of the QTLs contributing
777 to this variation, that is, most traits are independent of the loci affecting segregation or fertility
778 in the F2 generations (Table S5).

779 Hybrid F2 offspring often exhibited phenotypic values beyond the range of the parental
780 lineages, particularly for plant height, rosette diameter, leaf length and flowering time. Indeed,
781 although the two parental genotypes did not differ in the timing of flowering, it was for this trait
782 that the largest QTL was detected on chromosome 8. Our study showed that changes in
783 flowering time in *A. nemorensis* and *A. sagittata* hybrids are not linked to the well-known genes
784 controlling flowering time, *FLC* or *CO* (reviewed in Alonso-Blanco *et al.*, 2009; Andrés &
785 Coupland, 2012). Instead, the fine-mapping of the largest QTL defined a genetic region that
786 contains only one candidate gene for flowering time. This gene, first described as *TFL1* in *A.*
787 *thaliana,* accelerates flowering by decreasing the number of vegetative side buds in this
788 species (Alvarez *et al.*, 1992; Moraes *et al.*, 2019). In the perennial species *A. alpina*, it further
789 interacts with the age pathway to prevent juvenile plants from responding to vernalization,

790 thereby controlling the transition out of the juvenile stage, an additional developmental
791 transition of central importance for perennials (Wang & Albani *et al.*, 2011). Because this
792 flowering time variant is independent from all segregation distortions and fertility alleles, it
793 appears as a potential adaptive trait likely to be reshaped as a result of gene flow. Studies of
794 flowering time provided some of the most remarkable examples of contemporary adaptation
795 to climate change in plants (Hancock *et al.*, 2024 submitted), and adaptive introgression of
796 flowering time alleles have been documented in several cases (Le Corre *et al.*, 2002; Todesco
797 *et al.*, 2020; Wang *et al.*, 2021). Environmental responses to global climate change include
798 advancing flowering time: many plants induce earlier flowering as a strategy to escape warmer
799 temperatures (e.g., Anderson *et al.*, 2012; Cai *et al.*, 2019; Siegmund *et al.*, 2016; Tun *et al.*,
800 2021).

801 Which additional, genetically different traits may be adaptive in natural communities remains
802 to be determined. Larger leaves, greater lateral spread and lower specific leaf area, all of
803 which are variable in the descendants of hybrid individuals in this system, have been
804 associated with competitive advantage in the ephemeral wetland of vernal pool plant
805 communities (Kraft *et al.*, 2015). Interestingly, the *A. nemorensis* maternal background
806 increased rosette diameter, especially at early stages, while the *A. sagittata* maternal
807 background increased stem leaf length. Both of these traits can improve light capture, but their
808 relative fitness relevance should depend on the trade-off between survival and competition
809 (Lundgren & Des Marais, 2020). Backcrossing of *A. nemorensis* pollen on *A. sagittata* mother
810 plants appeared to occur more frequently among hybrids (Dittberner *et al.*, 2019; Dittberner *et*
811 *al.*, 2022), which would thus promote an increase in stem leaf length. Therefore, genetic and
812 maternal variants may contribute to the emergence of a particularly competitive genotype in
813 the dense plant communities of floodplain meadows. In this context, it is intriguing that
814 signatures of putative selective sweeps in the parental species were found for many of the
815 QTLs determining variation among rosette size. Recent selection in the parental lineages
816 however, has not been systematically associated with variable QTLs, so that much of the
817 variation manifested in the F2 generation forms a new base of variants that has not yet been
818 shaped by natural selection.

819 As the climate changes and land-use intensifies, the native floodplain habitat is increasingly
820 exposed to drought events as well as flooding, both of which will affect plant survival in natural
821 environments and neither of which could be quantified in this common garden experiment
822 (Colloff *et al.*, 2016). In situ analyses of the performance of hybrid offspring are therefore
823 needed to shed light on the genetic basis of variation in survival rates. We conclude that there
824 is sufficient genetic diversity in our system for hybridization to generate novelty. The prospects

825 of hybridization between these species, however, will depend on how selective pressures act
826 on genetically variable traits within the architecture of allelic transmission.

827 **Acknowledgments**

828 This work was supported by the Deutsche Forschungsgemeinschaft (DFG [ME2742/13-1,
829 TRR341 and EXC 2048/1–390686111). We thank the Cologne Center for Genomics (CCG),
830 the Regionales Rechenzentrum der Universität zu Köln (RRZK), the German Network for
831 Bioinformatics Infrastructure (de.NBI) and ELIXIR-DE (Forschungszentrum Jülich and W-
832 de.NBI-001, W-de.NBI-004, W-de.NBI-008, W-de.NBI-010, W-de.NBI-013, W-de.NBI-014, W-
833 de.NBI-016, W-de.NBI-022). We thank K. Schneeberger, B. Hüttel, A. Hancock, M. Stetter, I.
834 Calic and M. Hajheidari for valuable feedback. This work benefited from the contribution of Y.
835 Özoglan to data collection.

836 **Competing interests**

837 None declared.

838 **Author contributions**

839 N.R. designed and performed the RADseq and QTL mapping analyses, conducted flowering-
840 time experiments and analyses, and wrote the manuscript. L.M. contributed to the whole-
841 genome sequencing (WGS) analyses and wrote the WGS section of the manuscript. L.H.
842 assisted with RADseq data analysis. K.K. assisted with genotype correction. A.S.K. generated
843 the genome annotations. T.A., C.I.D., S.A., R.Y.W, and N.R. generated the genome
844 assemblies. G.S. and B. S. contributed to data interpretation. A.T. and J.d.M. conceived and
845 supervised the project, contributed to data interpretation, and reviewed and edited the
846 manuscript.

847 **Data Availability**

848 FASTQ files of the F2 population, genome assemblies, and annotations are available at the
849 European Nucleotide Archive (ENA) under project number [PRJEB89863]. All supplementary
850 figures can be found at Supplementary Figures. All scripts, VCF file, and phenotypic datasets
851 used in this study are available on GitHub via the following links:

852 - Suppl. File 1. Phenotypic analyses:

853 https://github.com/nedarahnama/Contemporary_hybridization/tree/master/01_phenotypic
854 _analyses

855 - Suppl. File 2. Genome assembly:

https://github.com/nedarahnama/Contemporary_hybridization/tree/master/02_genome_assembly

- Suppl. File 3. RADseq analysis:

https://github.com/nedarahnama/Contemporary_hybridization/tree/master/03_rad_seq

- Suppl. File 4. Genetic map construction:

https://github.com/nedarahnama/Contemporary_hybridization/tree/master/04_genetic_map

- Suppl. File 5. QTL mapping analysis:

https://github.com/nedarahnama/Contemporary_hybridization/tree/master/05_qtl_mapping

- Suppl. File 6. Flowering time fine-mapping analysis:

https://github.com/nedarahnama/Contemporary_hybridization/tree/master/06_fine_mapping

- Suppl. File 7. Sweep detection:

https://github.com/Luker121/OverlapSweepQTL/tree/main

885 ## References

886 **Abbott RJ**. **2017**. Plant speciation across environmental gradients and the occurrence and nature of
887 hybrid zones. *Journal of Systematics and Evolution* **55**.

888 **Abbott R, Albach D, Ansell S, Arntzen JW, Baird SJE, Bierne N, Boughman J, Brelsford A, Buerkle CA,**
889 **Buggs R, *et al.* 2013**. Hybridization and speciation. *Journal of Evolutionary Biology* **26**.

890 **Alachiotis N, Stamatakis A, Pavlidis P**. **2012**. OmegaPlus: A scalable tool for rapid detection of
891 selective sweeps in whole-genome datasets. *Bioinformatics* **28**.

892 **Albani MC, Castaings L, Wötzel S, Mateos JL, Wunder J, Wang R, Reymond M, Coupland G**. **2012**.
893 PEP1 of *Arabis alpina* Is Encoded by Two Overlapping Genes That Contribute to Natural Genetic
894 Variation in Perennial Flowering. *PLoS Genetics* **8**.

895 **Alcázar R, von Reth M, Bautor J, Chae E, Weigel D, Koornneef M, Parker JE**. **2014**. Analysis of a Plant
896 Complex Resistance Gene Locus Underlying Immune-Related Hybrid Incompatibility and Its
897 Occurrence in Nature. *PLoS Genetics* **10**.

898 **Alonge M, Lebeigle L, Kirsche M, Jenike K, Ou S, Aganezov S, Wang X, Lippman ZB, Schatz MC, Soyk**
899 **S**. **2022**. Automated assembly scaffolding using RagTag elevates a new tomato system for high-
900 throughput genome editing. *Genome Biology* **23**.

901 **Alonso-Blanco C, Aarts MGM, Bentsink L, Keurentjes JJB, Reymond M, Vreugdenhil D, Koornneef M**.
902 **2009**. What has natural variation taught us about plant development, physiology, and adaptation?
903 *Plant Cell* **21**.

904 **Alvarez J, Guli CL, Yu X -H, Smyth DR**. **1992**. terminal flower: a gene affecting inflorescence
905 development in *Arabidopsis thaliana*. *The Plant Journal* **2**.

906 **Anderson JT, Panetta AM, Mitchell-Olds T**. **2012**. Evolutionary and Ecological Responses to
907 Anthropogenic Climate Change. *Plant Physiology* **160**: 1728–1740.

908 **Anderson E, Stebbins GL**. **1954**. HYBRIDIZATION AS AN EVOLUTIONARY STIMULUS. *Evolution* **8**.

909 **Andrés F, Coupland G**. **2012**. The genetic basis of flowering responses to seasonal cues. *Nature*
910 *Reviews Genetics* **13**.

911 **Andrews S**. **2010**. FastQC: a quality control tool for high throughput sequence data. 2010.
912 *Https://Www.Bioinformatics.Babraham.Ac.Uk/Projects/Fastqc/*.

913 **Aronen T, Nikkanen T, Harju A, Tiimonen H, Häggman H**. **2002**. Pollen competition and seed-siring
914 success in *Picea abies*. *Theoretical and Applied Genetics* **104**.

915 **Becker M, Gruenheit N, Steel M, Voelckel C, Deusch O, Heenan PB, McLenachan PA, Kardailsky O,**
916 **Leigh JW, Lockhart PJ**. **2013**. Hybridization may facilitate in situ survival of endemic species through
917 periods of climate change. *Nature Climate Change* **3**.

918 **Blanckaert A, Sriram V, Bank C**. **2023**. In search of the Goldilocks zone for hybrid speciation II: hard
919 times for hybrid speciation? *Evolution* **77**.

920 **Bomblies K, Weigel D**. **2007**. Hybrid necrosis: Autoimmunity as a potential gene-flow barrier in plant
921 species. *Nature Reviews Genetics* **8**.

Bontrager M, Angert AL. **2019**. Gene flow improves fitness at a range edge under climate change. *Evolution Letters* **3**.

Brauer CJ, Sandoval-Castillo J, Gates K, Hammer MP, Unmack PJ, Bernatchez L, Beheregaray LB. **2023**. Natural hybridization reduces vulnerability to climate change. *Nature Climate Change* **13**.

Broman KW, Wu H, Sen Ś, Churchill GA. **2003**. R/qtl: QTL mapping in experimental crosses. *Bioinformatics* **19**.

Buerkle CA, Morris RJ, Asmussen MA, Rieseberg LH. **2000**. The likelihood of homoploid hybrid speciation. *Heredity* **84**.

Burmeier S, Eckstein RL, Donath TW, Otte A. **2011**. Plant pattern development during early post-restoration succession in grasslands-a case study of *Arabis nemorensis*. *Restoration Ecology* **19**.

Cai Z, Zhou L, Ren NN, Xu X, Liu R, Huang L, Zheng XM, Meng QL, Du YS, Wang MX, *et al.* 2019. Parallel Speciation of Wild Rice Associated with Habitat Shifts. *Molecular Biology and Evolution* **36**.

Carey K, Ganders FR. **1980**. Heterozygote Advantage at the Fruit Wing Locus in *Plectritis congesta* (Valerianaceae). *Evolution* **34**.

Catchen J, Hohenlohe PA, Bassham S, Amores A, Cresko WA. **2013**. Stacks: An analysis tool set for population genomics. *Molecular Ecology* **22**.

Ceballos G, Ehrlich PR, Raven PH. **2020**. Vertebrates on the brink as indicators of biological annihilation and the sixth mass extinction. *Proceedings of the National Academy of Sciences* **117**: 13596–13602.

Cerise M, da Silveira Falavigna V, Rodríguez-Maroto G, Signol A, Severing E, Gao H, van Driel A, Vincent C, Wilkens S, Iacobini FR, *et al.* 2023. Two modes of gene regulation by *TFL1* mediate its dual function in flowering time and shoot determinacy of *Arabidopsis*. *Development (Cambridge)* **150**.

Cheng H, Concepcion GT, Feng X, Zhang H, Li H. **2021**. Haplotype-resolved de novo assembly using phased assembly graphs with hifiasm. *Nature Methods* **18**.

Cheng H, Jarvis ED, Fedrigo O, Koepfli KP, Urban L, Gemmell NJ, Li H. **2022**. Haplotype-resolved assembly of diploid genomes without parental data. *Nature Biotechnology*.

Chettoor AM, Givan SA, Cole RA, Coker CT, Unger-Wallace E, Vejlupkova Z, Vollbrecht E, Fowler JE, Evans MMS. **2014**. Discovery of novel transcripts and gametophytic functions via RNA-seq analysis of maize gametophytic transcriptomes. *Genome Biology* **15**.

Chunco AJ. **2014**. Hybridization in a warmer world. *Ecology and Evolution* **4**.

Clarke HJ, Khan TN, Siddique KHM. **2004**. Pollen selection for chilling tolerance at hybridisation leads to improved chickpea cultivars. *Euphytica* **139**.

Clo J, Ronfort J, Gay L. **2021**. Fitness consequences of hybridization in a predominantly selfing species: insights into the role of dominance and epistatic incompatibilities. *Heredity* **127**.

Cochrane SKJ, Andersen JH, Berg T, Blanchet H, Borja A, Carstensen J, Elliott M, Hummel H, Niquil N, Renaud PE. **2016**. What is marine biodiversity? Towards common concepts and their implications for assessing biodiversity status. *Frontiers in Marine Science* **3**.

Colloff MJ, Lavorel S, Wise RM, Dunlop M, Overton IC, Williams KJ. **2016**. Adaptation services of floodplains and wetlands under transformational climate change. *Ecological Applications* **26**.

Cooper BS, Sedghifar A, Nash WT, Comeault AA, Matute DR. **2018**. A Maladaptive Combination of Traits Contributes to the Maintenance of a *Drosophila* Hybrid Zone. *Current Biology* **28**.

[Core Writing Team HL and JR (eds.). **2022**. Climate Change 2023: Synthesis Report. Contribution of Working Groups I, II and III to the Sixth Assessment Report of the Intergovernmental Panel on Climate Change. *IPCC* **13**.

Le Corre V, Roux F, Reboud X. **2002**. DNA polymorphism at the *FRIGIDA* gene in *Arabidopsis thaliana*: Extensive nonsynonymous variation is consistent with local selection for flowering time. *Molecular Biology and Evolution* **19**.

Coughlan JM, Matute DR. **2020**. The importance of intrinsic postzygotic barriers throughout the speciation process: Intrinsic barriers throughout speciation. *Philosophical Transactions of the Royal Society B: Biological Sciences* **375**.

Cowie RH, Bouchet P, Fontaine B. **2022**. The Sixth Mass Extinction: fact, fiction or speculation? *Biological Reviews* **97**.

Danecek P, Auton A, Abecasis G, Albers CA, Banks E, DePristo MA, Handsaker RE, Lunter G, Marth GT, Sherry ST, *et al.* 2011. The variant call format and VCFtools. *Bioinformatics* **27**.

Delaneau O, Marchini J, McVeanh GA, Donnelly P, Lunter G, Myers S, Gupta-Hinch A, Iqbal Z, Mathieson I, Rimmer A, *et al.* 2014. Integrating sequence and array data to create an improved 1000 Genomes Project haplotype reference panel. *Nature Communications* **5**.

Delaneau O, Ongen H, Brown AA, Fort A, Panousis NI, Dermitzakis ET. **2017**. A complete tool set for molecular QTL discovery and analysis. *Nature Communications* **8**.

Dittberner H, Becker C, Jiao WB, Schneeberger K, Hölzel N, Tellier A, de Meaux J. **2019**. Strengths and potential pitfalls of hay transfer for ecological restoration revealed by RAD-seq analysis in floodplain *Arabis* species. *Molecular Ecology* **28**.

Dittberner H, Tellier A, De Meaux J. **2022**. Approximate Bayesian Computation Untangles Signatures of Contemporary and Historical Hybridization between Two Endangered Species. *Molecular Biology and Evolution* **39**.

Dobzhansky T. **1936**. STUDIES ON HYBRID STERILITY. II. LOCALIZATION OF STERILITY FACTORS IN DROSOPHILA PSEUDOOBSCURA HYBRIDS. *Genetics* **21**.

Domínguez E, Cuartero J, Fernández-Muñoz R. **2005**. Breeding tomato for pollen tolerance to low temperatures by gametophytic selection. *Euphytica* **142**.

Durand NC, Robinson JT, Shamim MS, Machol I, Mesirov JP, Lander ES, Aiden EL. 2016a. *Cell Systems* **3: 99–101**.

Durand NC, Shamim MS, Machol I, Rao SS, Huntley MH, Lander ES, Aiden EL. 2016b. *Cell Systems* **3: 95–98.**

Eichenberg D, Bowler DE, Bonn A, Bruelheide H, Grescho V, Harter D, Jandt U, May R, Winter M, Jansen F. **2021**. Widespread decline in Central European plant diversity across six decades. *Global Change Biology* **27**.

Ellstrand NC, Schierenbeck KA. **2000**. Hybridization as a stimulus for the evolution of invasiveness in plants? *Proceedings of the National Academy of Sciences of the United States of America* **97**.

Finseth F. **2023**. Female meiotic drive in plants: mechanisms and dynamics. *Current Opinion in Genetics and Development* **82**.

Finseth FR, Dong Y, Saunders A, Fishman L. **2015**. Duplication and adaptive evolution of a key centromeric protein in mimulus, a genus with female meiotic drive. *Molecular Biology and Evolution* **32**.

Fishman L, Kelly JK. **2015**. Centromere-associated meiotic drive and female fitness variation in *Mimulus*. *Evolution* **69**.

Frankham R. **2015**. Genetic rescue of small inbred populations: meta-analysis reveals large and consistent benefits of gene flow. *Molecular Ecology* **24**.

Goulet BE, Roda F, Hopkins R. **2017**. Hybridization in plants: Old ideas, new techniques[OPEN]. *Plant Physiology* **173**.

Haley CS, Knott SA. **1992**. A simple regression method for mapping quantitative trait loci in line crosses using flanking markers. *Heredity* **69**.

Haller BC, Galloway J, Kelleher J, Messer PW, Ralph PL. **2019**. Tree-sequence recording in SLiM opens new horizons for forward-time simulation of whole genomes. *Molecular Ecology Resources* **19**.

Haller BC, Messer PW. **2023**. SLiM 4: Multispecies Eco-Evolutionary Modeling. *American Naturalist* **201**.

Hancock A, Portalier S, Fulgione A, Stetter MG, de Meaux J. **2024**. The molecular basis of adaptation to climatic factors and range change in plants. Annual reviews in Ecology and Evolution. *Submitted*.

Hansen MM, Olivieri I, Waller DM, Nielsen EE. **2012**. Monitoring adaptive genetic responses to environmental change. *Molecular Ecology* **21**.

Hölzel N. **2005**. Seedling recruitment in flood-meadow species: The effects of gaps, litter and vegetation matrix. *Applied Vegetation Science* **8**.

Hooper JNA, Kennedy JA, Quinn RJ. **2002**. Biodiversity 'hotspots', patterns of richness and endemism, and taxonomic affinities of tropical Australian sponges (Porifera). *Biodiversity and Conservation* **11**.

Hopkins R. **2013**. Reinforcement in plants. *New Phytologist* **197**.

Karl R, Koch MA. **2014**. Phylogenetic signatures of adaptation: The *Arabis hirsuta* species aggregate (Brassicaceae) revisited. *Perspectives in Plant Ecology, Evolution and Systematics* **16**.

Klepikova A V., Kasianov AS, Gerasimov ES, Logacheva MD, Penin AA. **2016**. A high resolution map of the *Arabidopsis thaliana* developmental transcriptome based on RNA-seq profiling. *Plant Journal* **88**.

Kraft TS, Wright SJ, Turner I, Lucas PW, Oufiero CE, Supardi Noor MN, Sun IF, Dominy NJ. **2015**. Seed size and the evolution of leaf defences. *Journal of Ecology* **103**.

Lankinen S, Maad J, Armbruster WS. **2009**. Pollen-tube growth rates in *Collinsia heterophylla* (Plantaginaceae): One-donor crosses reveal heritability but no effect on sporophytic-offspring fitness. *Annals of Botany* **103**.

1036 **Lewontin RC, Birch LC**. **1966**. Hybridization as a Source of Variation for Adaptation to New
1037 Environments. *Evolution* **20**.

1038 **Li H, Durbin R**. **2009**. Fast and accurate short read alignment with Burrows-Wheeler transform.
1039 *Bioinformatics* **25**.

1040 **Li H, Handsaker B, Wysoker A, Fennell T, Ruan J, Homer N, Marth G, Abecasis G, Durbin R**. **2009**. The
1041 Sequence Alignment/Map format and SAMtools. *Bioinformatics* **25**.

1042 **Li J, Schumer M, Bank C**. **2022**. Imbalanced segregation of recombinant haplotypes in hybrid
1043 populations reveals inter- and intrachromosomal Dobzhansky-Muller incompatibilities. *PLoS Genetics*
1044 **18**.

1045 **Lundgren MR, Des Marais DL**. **2020**. Life History Variation as a Model for Understanding Trade-Offs in
1046 Plant–Environment Interactions. *Current Biology* **30**.

1047 **Ma Y, Marczewski T, Xue D, Wu Z, Liao R, Sun W, Marczewski J**. **2019**. Conservation implications of
1048 asymmetric introgression and reproductive barriers in a rare primrose species. *BMC Plant Biology* **19**.

1049 **Malik HS**. **2005**. *Mimulus* finds centromeres in the driver's seat. *Trends in Ecology and Evolution* **20**.

1050 **Mallet J**. **2007**. Hybrid speciation. *Nature* **446**: 279–283.

1051 **Marçais G, Kingsford C**. **2011**. A fast, lock-free approach for efficient parallel counting of occurrences
1052 of k-mers. *Bioinformatics* **27**: 764–770.

1053 **Martin M**. **2011**. Cutadapt removes adapter sequences from high-throughput sequencing reads.
1054 *EMBnet.journal* **17**.

1055 **Masly JP, Presgraves DC**. **2007**. High-resolution genome-wide dissection of the two rules of speciation
1056 in *Drosophila*. *PLoS Biology* **5**.

1057 **Mathar W, Kleinebecker T, Hölzel N**. **2015**. Environmental variation as a key process of co-existence
1058 in flood-meadows. *Journal of Vegetation Science* **26**.

1059 **McKenna A, Hanna M, Banks E, Sivachenko A, Cibulskis K, Kernytsky A, Garimella K, Altshuler D,**
1060 **Gabriel S, Daly M, *et al.* 2010**. The genome analysis toolkit: A MapReduce framework for analyzing
1061 next-generation DNA sequencing data. *Genome Research* **20**.

1062 **Moore JS, Hendry AP**. **2009**. Can gene flow have negative demographic consequences? Mixed
1063 evidence from stream threespine stickleback. *Philosophical Transactions of the Royal Society B:*
1064 *Biological Sciences* **364**.

1065 **Moraes TS, Dornelas MC, Martinelli AP**. **2019**. *FT*/*TFL1*: Calibrating plant architecture. *Frontiers in*
1066 *Plant Science* **10**.

1067 **Moran BM, Payne CY, Powell DL, Iverson ENK, Donny AE, Banerjee SM, Langdon QK, Gunn TR,**
1068 **Rodriguez-Soto RA, Madero A, *et al.* 2024**. A lethal mitonuclear incompatibility in complex I of natural
1069 hybrids. *Nature* **626**.

1070 **Muller HJ**. **1942**. Isolating mechanisms, evolution and temperature. *Biol. Symp* **6**.

1071 **Nocchi G, Wang J, Yang L, Ding J, Gao Y, Buggs RJA, Wang N**. **2023**. Genomic signals of local adaptation
1072 and hybridization in Asian white birch. *Molecular Ecology* **32**.

Okonechnikov K, Conesa A, García-Alcalde F. **2016**. Qualimap 2: Advanced multi-sample quality control for high-throughput sequencing data. *Bioinformatics* **32**.

Parker MT, Amar S, Campoy JA, Krause K, Tusso S, Marek M, Huettel B, Schneeberger K. **2025**. Scalable eQTL mapping using single-nucleus RNA-sequencing of recombined gametes from a small number of individuals. *PLOS Biology* **23**.

Peñalba J V., Runemark A, Meier JI, Singh P, Wogan GOU, Sánchez-Guillén R, Mallet J, Rometsch SJ, Menon M, Seehausen O, *et al.* 2024. The Role of Hybridization in Species Formation and Persistence. *Cold Spring Harbor Perspectives in Biology*.

Pfennig KS, Kelly AL, Pierce AA. **2016**. Hybridization as a facilitator of species range expansion. *Proceedings of the Royal Society B: Biological Sciences* **283**.

Pinkas R, Zamir D, Ladizinsky G. **1985**. Allozyme divergence and evolution in the genusLens. *Plant Systematics and Evolution* **151**: 131–140.

Powell DL, García-Olazábal M, Keegan M, Reilly P, Du K, Díaz-Loyo AP, Banerjee S, Blakkan D, Reich D, Andolfatto P, *et al.* 2020. Natural hybridization reveals incompatible alleles that cause melanoma in swordtail fish. *Science* **368**.

Presgraves DC. **2010**. The molecular evolutionary basis of species formation. *Nature Reviews Genetics* **11**.

Ranallo-Benavidez TR, Jaron KS, Schatz MC. **2020**. GenomeScope 2.0 and Smudgeplot for reference-free profiling of polyploid genomes. *Nature Communications* **11**.

Rhymer JM, Simberloff D. **1996**. Extinction by hybridization and introgression. *Annual Review of Ecology and Systematics* **27**.

Rieseberg LH, Raymond O, Rosenthal DM, Lai Z, Livingstone K, Nakazato T, Durphy JL, Schwarzbach AE, Donovan LA, Lexer C. **2003**. Major ecological transitions in wild sunflowers facilitated by hybridization. *Science* **301**.

Rivera-Colón AG, Catchen J. **2022**. Population Genomics Analysis with RAD, Reprised: Stacks 2. In: Methods in Molecular Biology.

Rosser N, Seixas F, Queste LM, Cama B, Mori-Pezo R, Kryvokhyzha D, Nelson M, Waite-Hudson R, Goringe M, Costa M, *et al.* 2024. Hybrid speciation driven by multilocus introgression of ecological traits. *Nature* **628**: 811–817.

Rutley N, Twell D. **2015**. A decade of pollen transcriptomics. *Plant Reproduction* **28**.

Sandler L, Novitski E. **1957**. Meiotic Drive as an Evolutionary Force. *The American Naturalist* **91**.

Schlaepfer MA, Lawler JJ. **2023**. Conserving biodiversity in the face of rapid climate change requires a shift in priorities. *Wiley Interdisciplinary Reviews: Climate Change* **14**.

Schnittler M, Günther KF. **1999**. Central European vascular plants requiring priority conservation measures - An analysis from national Red Lists and distribution maps. *Biodiversity and Conservation* **8**.

Schumer M, Brandvain Y. **2016**. Determining epistatic selection in admixed populations. *Molecular ecology* **25**.

1110 **Schumer M, Cui R, Powell DL, Dresner R, Rosenthal GG, Andolfatto P**. **2014**. High-resolution mapping
1111 reveals hundreds of genetic incompatibilities in hybridizing fish species. *eLife* **2014**.

1112 **Schumer M, Cui R, Rosenthal GG, Andolfatto P**. **2015**. Reproductive Isolation of Hybrid Populations
1113 Driven by Genetic Incompatibilities. *PLoS Genetics* **11**.

1114 **Schumer M, Xu C, Powell DL, Durvasula A, Skov L, Holland C, Blazier JC, Sankararaman S, Andolfatto**
1115 **P, Rosenthal GG, *et al.* 2018**. Natural selection interacts with recombination to shape the evolution of
1116 hybrid genomes. *Science* **360**.

1117 **Seehausen O**. **2004**. Hybridization and adaptive radiation. *Trends in Ecology and Evolution* **19**.

1118 **Siegmund JF, Wiedermann M, Donges JF, Donner R V. 2016**. Impact of temperature and precipitation
1119 extremes on the flowering dates of four German wildlife shrub species. *Biogeosciences* **13**.

1120 **Sim SB, Corpuz RL, Simmonds TJ, Geib SM**. **2022**. HiFiAdapterFilt, a memory efficient read processing
1121 pipeline, prevents occurrence of adapter sequence in PacBio HiFi reads and their negative impacts on
1122 genome assembly. *BMC Genomics* **23**.

1123 **Simons YB, Sella G**. **2016**. The impact of recent population history on the deleterious mutation load
1124 in humans and close evolutionary relatives. *Current Opinion in Genetics and Development* **41**.

1125 **Smit AFA, Hubley R, Grenn P**. **2015**. RepeatMasker Open-4.0. *RepeatMasker Open-4.0.7.*

1126 **Smith LM, Bomblies K, Weigel D**. **2011**. Complex evolutionary events at a tandem cluster of
1127 *Arabidopsis thaliana* genes resulting in a single-locus genetic incompatibility. *PLoS Genetics* **7**.

1128 **Snow AA, Spira TP**. **1996**. Pollen-tube competition and male fitness in *Hibiscus moscheutos*. *Evolution*
1129 **50**.

1130 **Staudinger MD, Grimm NB, Staudt A, Carter SF, Chapin FS, Kareiva P, Ruckelshaus M, Stein BA**. **2012**.
1131 Impacts of climate change on biodiversity, ecosystems, and ecosystem services: technical input to the
1132 2013 National Climate Assessment. *Cooperative Report to the 2013 National Climate Assessment*.

1133 **Stull GW, Pham KK, Soltis PS, Soltis DE**. **2023**. Deep reticulation: the long legacy of hybridization in
1134 vascular plant evolution. *Plant Journal* **114**.

1135 **Taylor J, Butler D**. **2017**. R package ASMap: Efficient genetic linkage map construction and diagnosis.
1136 *Journal of Statistical Software* **79**.

1137 **Theissinger K, Fernandes C, Formenti G, Bista I, Berg PR, Bleidorn C, Bombarely A, Crottini A, Gallo**
1138 **GR, Godoy JA, *et al.* 2023**. How genomics can help biodiversity conservation. *Trends in Genetics* **39**.

1139 **Titz W**. **1979**. Die Interfertilitätsbeziehungen europäischer Sippen der *Arabis hirsuta*-Gruppe
1140 (Brassicaceae). *Plant Systematics and Evolution* **131**.

1141 **Todesco M, Owens GL, Bercovich N, Légaré JS, Soudi S, Burge DO, Huang K, Ostevik KL, Drummond**
1142 **EBM, Imerovski I, *et al.* 2020**. Massive haplotypes underlie ecotypic differentiation in sunflowers.
1143 *Nature* **584**.

1144 **Todesco M, Pascual MA, Owens GL, Ostevik KL, Moyers BT, Hübner S, Heredia SM, Hahn MA, Caseys**
1145 **C, Bock DG, *et al.* 2016**. Hybridization and extinction. *Evolutionary Applications* **9**.

1146 **Tun W, Yoon J, Jeon JS, An G**. **2021**. Influence of Climate Change on Flowering Time. *Journal of Plant*
1147 *Biology* **64**.

Villasenor Alva JA, Estrada EG. **2009**. A generalization of Shapiro-Wilk's test for multivariate normality. *Communications in Statistics - Theory and Methods* **38**.

Wang R, Albani MC, Vincent C, Bergonzi S, Luan M, Bai Y, Kiefer C, Castillo R, Coupland G. **2011**. Aa tfl1 confers an age-dependent response to vernalization in perennial *Arabis alpina*. *Plant Cell* **23**.

Wang Z, Jiang Y, Bi H, Lu Z, Ma Y, Yang X, Chen N, Tian B, Liu B, Mao X, *et al.* 2021. Hybrid speciation via inheritance of alternate alleles of parental isolating genes. *Molecular Plant* **14**.

Wang RJ, White MA, Payseur BA. **2015**. The Pace of hybrid incompatibility evolution in house mice. *Genetics* **201**.

White MA, Steffy B, Wiltshire T, Payseur BA. **2011**. Genetic dissection of a key reproductive barrier between nascent species of house mice. *Genetics* **189**.

White MA, Stubbings M, Dumont BL, Payseur BA. **2012**. Genetics and evolution of hybrid male sterility in house mice. *Genetics* **191**.

Wickham H. **2011**. ggplot2. *Wiley Interdisciplinary Reviews: Computational Statistics* **3**: 180–185.

Zuellig MP, Sweigart AL. **2018**. Gene duplicates cause hybrid lethality between sympatric species of *Mimulus*. *PLoS Genetics* **14**.